의학박사 학위논문

Effects of Bioactive Whitlockite-Based Biomaterials on Bone Regeneration in Bone Defect and Osteonecrosis Models

-Studies on the Development of Functional Bone Cement and Antioxidant-Coated Scaffold-

생체활성 휘트로카이트계 생체재료가 골 결손 및 괴사 모델에서 골 재생에 미치는 영향

-기능성 골시멘트와 항산화 코팅 지지체 개발에 대한 연구-

2023년 8월

서울대학교 대학원

의학과 정형외과 전공

QuanZhe Liu

Ph.D. Dissertation of Medicine

Effects of Bioactive Whitlockite-Based Biomaterials on Bone Regeneration in Bone Defect and Osteonecrosis Models.

-Studies on the Development of Functional Bone Cement and Antioxidant-Coated Scaffold-

August 2023

Graduate School of Medicine

Seoul National University

Orthopedic Surgery Major

Name : QuanZhe Liu

생체활성 휘트로카이트계 생체재료가 골 결손 및 괴사 모델에서 골 재생에 미치는 영향

－기능성 골시멘트와 항산화 코팅 지지체 개발에 대한 연구－

지도교수 이 재 협

이 논문을 의학박사 학위논문으로 제출함

2023년 4월

서울대학교 대학원

의학과 정형외과 전공

류치엔저

류치엔저의 박사 학위논문을 인준함

2023년 7월

위 원 장	조 현 철	(인)
부 위 원 장	이 재 협	(인)
위 원	박 민 현	(인)
위 원	박 지 웅	(인)
위 원	김 영 훈	(인)

Abstract

Effects of Bioactive Whitlockite-Based Biomaterials on Bone Regeneration in Bone Defect and Osteonecrosis Models.

-Studies on the Development of Functional Bone Cement and Antioxidant-Coated Scaffold-

QuanZhe Liu

Department of Orthopedic Surgery

The Graduate School

Seoul National University

Background:

Whitlockite (WH: Ca18Mg2(HPO4)2(PO4)12) has outstanding advantages and potential as a new bio-ceramic. Compared with Calcium phosphate-based ceramics, WH is of great significance in bone tissue regeneration engineering because its chemical composition contains magnesium ions in addition to calcium and phosphate ions. In previous studies, WH showed better osteoconductivity and osseointegration than hydroxyapatite (HAP) and tricalcium phosphate (TCP), and it was more effective in promoting bone regeneration. However, preclinical studies to demonstrate the potential clinical value of WH ceramic materials and biomaterials based on them are still lacking. Therefore, this study aims to design and fabricate WH-based biomaterials for specific bone diseases, reveal their biological properties, and verify the application value and potential as new bioceramics and biomaterials

through in vitro and in vivo experiments.

Methods:

This study designed and fabricated two types of WH-based customized biomaterials for clinically common bone disease (osteoporotic vertebral compression fracture and osteonecrosis of the femoral head). That is WH-incorporated functional bone cement (Part 1) and antioxidant-coated multifunctional WH scaffold (Part 2). In part 1, Tetracalcium phosphate (TTCP) and WH were incorporated with Polymethyl methacrylate (PMMA) bone cement to prepare a novel functional bone cement (TTCP/WH) and systemically evaluated its characteristics such as the operational working time and mechanical properties, etc., and compared with the International Standardization Organization standard (ISO 5833). And the biocompatibility, osteoconductivity, and osseointegration ability were evaluated through in vitro and in vivo studies. In part 2. First, following the Preferred Reporting Items for Systemic Reviews and Meta-analyses for Network Meta-analysis (PRISMA-NMA) reporting guideline, statistical analysis was performed on various early treatment methods for femoral head necrosis to evaluate their effectiveness. Then, the scaffold was designed and fabricated to treat femoral head necrosis using the tyrosinase immobilized glass bead (ImTYR) system as an antioxidant multifunctional whitlockite (WH) scaffold. Its physicochemical properties were systematically evaluated, and its biological properties were evaluated by in vitro study and animal experiments in a steroid-induced rabbit femoral head necrosis model.

Results:

In part 1, The TTCP/WH bone cement conformed to the ISO 5833 standard and showed a lower Young's modulus and suitable operational working time and physical properties for clinical use than conventional polymethylmethacrylate (PMMA). In vitro experiments showed that TTCP/WH bone cement exhibits good biocompatibility and osteogenic activity and improved expression of genes related to bone formation compared to the PMMA. and in rabbit ilium bone defect study, it showed stronger bone regeneration ability and osseointegration ability. In part 2. Results of the Network meta-analysis showed no statistical difference in the outcome of radiographic progression and conversion to total hip arthroplasty (THA), also in Harris Hip Score (HHS), other than core decompression(CD)+cell therapy showed relatively superior results in radiographic progression than nonsurgical treatment. And the osteoconductive scaffold containing WH was coated with antioxidant HA_CQ using the ImTYR system which provided a stable and safe method for coating medical devices with tyrosinase base reaction. In vitro experiments showed that WH and WH_CQ improved the osteogenic activity effect on human bone marrow stem cells(hBMSC) and the expression of genes related to bone formation compared to the control or collagen groups. In the steroid-induced osteonecrosis of femoral head(ONFH) rabbit model, WH and WH_CQ showed more distinct bone regeneration and microvascular regeneration capabilities than simple decompression, and a certain level of osteoclast inhibition. In addition, the WH_CQ group was found to have a positive effect on delaying the progression of osteonecrotic disease by reducing reactive oxygen species(ROS) and pro-inflammatory cytokine expression.

Conclusions:

TTCP/WH functional bone cement is expected to be a better choice for the treatment of osteoporotic vertebral compression fractures in the future due to its excellent biocompatibility, bone conductivity, and ability to promote bone formation. Antioxidant-coated multifunctional whitlockite scaffold possesses the unique biological properties of WH, so it has excellent bone regeneration ability, promotes the microvascular generation, and reduces ROS and pro-inflammation cytokine expression. It is expected to be a new idea and method for early treatment of the femoral head in the future.

The results of this study provide a deeper understanding and experimental basis for whitlockite ceramic-based biomaterials and are expected to be widely used in the medical field in the future.

Key Words: Whitlockite; Bio-ceramic; Bone Disease; Biomaterial; Bone Substitute;
Student Number: 2020-35192;

Contents

List of Tables

List of Figures

Chapter 1. Introduction

Calcium phosphate(CaP)-based ceramic is one of the widely used bone substitute materials in orthopedics which have been extensively studied, including hydroxyapatite (HAP)Ca10(PO4)6(OH)2[1,2]; tricalcium phosphate(TCP): Ca3 (PO4)2[3]; and their mixtures called biphasic calcium phosphates(BCP)[4-6]. It' s providing to be an excellent alternative material for load-bearing applications due to excellent bioactivity and biocompatibility as well as corrosion resistance, which is widely used in medical fields and the ultimate purpose of which is to repair and replace diseased and injured parts of the human body such as bones, joints, and teeth, etc.,[7,8]. Their advantages are undeniable, but, as an ideal bioceramic, there still are shortcomings that limit the scope of clinical applications.

HAP is one of the most investigated bioceramics in bone tissue engineering which can lead to positive influences on the adhesion and proliferation of osteoblasts because of its chemical composition same as the main bone components. But the slow degradation rate and poor mechanical strength as well as fracture toughness of pure HA hinder the complete bone formation and possibly increase the risk of infection[9]. And it also limited bioactivities in vitro and in vivo because of its chemical stability at body temperature and physiological PH[9,10]. On the other hand, β-TCP has been proven another common CaP ceramic that has better biodegradability than HAP. The main mechanism of bioactivity of TCP is partial dissolution and release of Ca and phosphate ions forming a biological apatite precipitate on the surface of the scaffold. And also bending strength and fracture toughness are reported better than those of

HAP but still lower than human cortical bone. It cannot be used for load-bearing implants and the degradation rate cannot match the growth rate of the new bone tissue[11].Against this background, whitlockite (WH: Ca18Mg2(HPO4)2(PO4)12) has recently received extensive attention and research as a novel bioceramic material which was the second most abundant mineral enriched with magnesium ions in human bone[12,13]. Compared with CaP ceramics, WH is characterized by the continuous supply of magnesium ions in addition to calcium and phosphate ions under physiological conditions[13], which plays a vital role in the normal function of the human musculoskeletal system. Mg is also a cofactor of hundreds of enzymes involved in lipids, and protein is essential to all living cells that can directly or indirectly affect osteogenesis, osteoclastogenesis, and angiogenesis[14]. WH was founded in bone with elevated dynamic loading[15] and involved in the early stages of bone regeneration by stimulating osteogenic differentiation, prohibiting osteoclastic activity, and transforming into mechanically enhanced bone tissue under physiological conditions[16], which provided great possibilities as a novel bioactive ceramic applicating in bone disease.

For example, polymethylmethacrylate (PMMA) bone cement, which is commonly used in osteoporotic compressive spinal fractures, does not directly bind to bone and has no biological activity. Apart from filling bone defects, there is no treatment for osteoporosis[17,18]. CaP-based bone cement is a suitable material for bone regeneration therapy because it resembles the mineral phase of bone and has a high similarity to bone tissue. but their brittle nature and poor mechanical properties limited application in loading-bearing locations[18]. Furthermore, for the early

treatment of avascular necrosis of the femoral head, many methods have been tried[19–21], including reducing internal pressure by drilling a hole in the bone and supplying nutrients to the hip joint by creating new blood vessels and added treatment such as autologous bone transplantation, stem cell transplantation or bone morphogenetic protein(BMP),etc., to alleviate the disease, but the effect is also insignificant. Therefore, new and effective treatment methods are still needed. In the previous study[12], our team validated with different animal bone defect models that WH as a better bone substitute material with better osteoconductivity compared with HAP and β−TCP can promote bone formation and faster migration of newly formed bone. And WH can also recapitulate bone regeneration by stimulating osteogenic differentiation, prohibiting osteoclastic activity by continuing the supply of PO43− and Mg2+[13].

Nonetheless, studies of WH application in specific bone disease models, whether in combination with other biomaterials or ceramics, are rarely reported, such as in osteoporosis or osteonecrosis. Therefore, the purpose of this study was to synthesize and prepare novel WH−based bioactive biomaterials for specific bone disease models and to evaluate their efficacy and potential clinical applications. This study was designed to be conducted in two parts: part 1: Preparation or synthesis of Mg−whitlockite incorporated functional bone cement for osteoporotic vertebral compression fracture. part 2: Preparation or synthesis of Whitlockite cross−linked collagen hyaluronic acid scaffold for early treatment of osteonecrosis of the femoral head. and evaluate their potential possibilities and advantages in specific bone disease models through in vitro and in vivo studies.

Chapter 2. Materials and Methods

Part 1. TTCP/WH-incorporated functional bone cement[22]

2.1.1 Material preparation and bone cement synthesis

The cement powder has components of PMMA, Barium sulfate, and calcium phosphate (TTCP, WH). Group TTCP and TTCP/WH (1:1 of wt %) have 40% of calcium phosphate in their powder. Whitlockite (Ca18Mg2(HPO4)2(PO4)12) powder was synthesized by the previously described wet precipitation method[13].

Cement was prepared by mixing cement powder and cement liquid in a 2:1 ratio. Cement powder contains 0.5% of benzoyl peroxide, and cement liquid contains N, N-dimethyl-p-toluidine, and hydroquinone. The cement liquid is mainly composed of Methyl methacrylate (MMA), and group 2,3,4 contains 20% of the total volume of Hydroxyethyl Methacrylate (HEMA) (**Figure 1, Table 1**). All Cement specimens were prepared in ambient conditions (22℃).

2.1.2 Physicochemical properties.

2.1.2.1 Temperature, Process time of bone cement during setting

3g of cement mixture was poured into the plastic mold (Ø=3.5cm, h=2cm). Wire-tip digital thermometer (testo 915i, Germany) was used for measuring temperature during the setting process. The temperature was recorded until it dropped 30% from the highest temperature. Process time was divided according to the cement's compressive strength. The first minute was given as mixing time. After mixing, cement was placed in a mold and measured surface strength by a tip-equipped Universal Testing Machine (UTM, Shimazu, EZ-SX STD) every 30 seconds.

Process time was divided into three zones Waiting time (0~5N), Injecting time (5~100N), and setting time (>100N) using measured surface strength.

2.1.2.2 Scanning electron microscopy and Mechanical strength test

Cement samples were fixed on specimen mount and platinum sputter coated. Scanning electron microscopy (FE-SEM, JSM-7800F Prime, JEOL Ltd, Japan) was used to take the microstructure images. Also, Energy dispersive spectroscopy (EDS) was used to analyze cement surface elements.

A tension & Compression tester (Instron 5582) was used for the mechanical testing of cement specimens. Specimens were prepared in ISO 5833 test size (Ø=6mm, h=12mm) and a compressive test was performed at 1mm/min of loading rate speed. Young's modulus was derived from the linear region of the strain-stress curve graph. For the 3-point bending strength test, (75mm) x (10mm) x (3.3mm) of cement specimens were fabricated. The compressive strength was measured until the specimen broke.

2.1.2.3 Chemical characteristics of bone cement

Bone cement specimens were prepared in the Ø=5mm, h=8mm size using plastic molds. Specimens were immersed in deionized water at a concentration of 0.1g/ml for 24 hours. Then, the supernatant of each sample was measured pH and ion concentration released from cement using an Inductively coupled plasma atomic emission spectrometer (ICPS-8100, Shimadzu).

2.1.3 In vitro study

2.1.3.1 Cell culture and viability

Human Bone marrow stem cells (hBMSC, ATCC, PCS-500-012) were seeded

(7500cells/cm^2, P4~P6) in the cell culture well plate with growth media (Dulbecco's modified eagle's medium (Hyclone) with 10% of FBS (Gibco), 1% of Penicillin-streptomycin) at 37℃, 5% CO2. Bone cement conditioned media was prepared as (0.1g of cement)/ (1ml of growth media) with Ø=5mm, h=8mm size cement scaffolds.

Before experiments, all specimens were autoclaved for sterilization.

Cell viability test conducted after 24hrs of hBMSCs culture with cement-conditioned media. Calcein AM and Ethidium homodimer-1 (Invitrogen) were used to mark the live/dead cells. Stained cells were imaged to calculate the viability of cells in conditioned media. Presto blue (Invitrogen) was used to measure the proliferation ratio of hBMSCs in cement-conditioned media. Every 24hrs, presto blue was treated into a cell culture plate with provided manufacturer's method. Cell proliferation ratio was calculated with relative fluorescence intensity as a day 0 control intensity was set to be 1.

2.1.3.2 hBMSC differentiation

hBMSCs were differentiated into the osteogenic and adipogenic lineage. Ascorbic acid-2-phosphate (50uM, A2P, Sigma), Glycerol-2-phosphate (10mM, G2P, Sigma), and Dexamethasone (100nM, Sigma), FBS (10%v/v) were mixed in growth cement conditioned media to make osteogenic medium. For the Adipogenic medium, Insulin (10ug/ml, Sigma), IBMX (0.5mM, Sigma), and Dexamethasone (1uM) were added to the growth media.

Cells were fixed with 4% Paraformaldehyde solution for 15min and washed with PBS. To identify differentiated cells, staining reagents were used. Naphthol AS-MX

(Sigma) for Alkaline phosphatase (ALP) staining, 2% of Alizarin red S (ARS, Sigma) for crystallized minerals in osteo-differentiated cells. And Oil red O (Sigma) was utilized for fat staining in adipo-differentiated cells.

2.1.3.3 Real-time PCR analysis

hBMSCs were differentiated for several time points (day 7,14,21) and total RNA was extracted. Total RNA was extracted by TRIZOL(Thermofisher) reagent according to the manufacturer's instructions. cDNA was synthesized with extracted RNA using an M-MLV cDNA synthesis kit (Enzynomics, Korea). Real-time PCR was conducted using synthesized cDNA and TOPreal SYBR green premix (Enzynomics) with StepOne Real-time PCR System (Thermofisher) to measure gene expression of differentiated cells. The primer sequence used in the study were: GAPDH (F: CGCTCTCTG CTCCTCCTGTT R: CCATGGTGTCTGAGCGATGT), ALP (F: ACGTGGCTAAGA ATGTCATC, R: CTGGTAGGCGATGTCCTTA), RUNX2 (F: TGGTTACTGTCATGGCGGGTA, R: TCTCAGATCGTTGAACCTTGCTA), COL1 (F: GTGCGATGACGTGATCTGTGA, R: CGGTGGTTTCTTGGTCGGT), PPAR-gamma (F: TACTGTCGGTTTCAGAAATGCC, R: GTCAGCGGACTCTGGATTCAG), CEBP-alpha (F: CCAGAAAGCTAGGTCGTGGGT, R: TGGACTGATCGTGCTTCGTGT), Adiponectin(F:AACATGCCCATTCGCTTTACC,R:TAGGCAAAGTAGTACAGCCCA).

2.1.4 In ex vivo study

2.1.4.1 Hemi-lumbar vertebrae preparation and demineralization

The 30 fresh-frozen Hemi-lumbar vertebrae from mature healthy pigs (weight 100 ±15kg) were prepared for testing by removing the intervertebral discs, soft tissue, and posterior and transverse elements. The demineralization procedure was carried

out as reported by Suk-JL[23]. The specimens were immersed in 1 N HCL (Duksan Pure Chemicals Co., Ansan, Korea) at room temperature until the bone mineral density (BMD) decreased by 35-40% (average 38%) as **Figure 2**. Then, it was washed with running distilled water and immersed in phosphate-buffered saline (Duksan Pure Chemicals Co., Ansan, Korea). A dual Energy X-ray Absorptiometry scan (Inalyzer, Medikors) was used to measure the Hemi-lumbar vertebrae BMD, and the value of BMD in the region of interest (ROI) was defined as vertebral body. The decalcified hemi-vertebrates were divided into four groups with seven samples in each group which had no statistical differences in volumetric BMD between the groups: group 1: PMMA, group 2: HEMA, group 3: TTCP. Group 4: TTCP/WH. All the operations were performed at a room temperature of 23±2℃, humidity: of 45% ±5% , and VAV(Variable Air Volume): of 100%.

2.1.4.2 Cement injection and operational working time

The operational working time was evaluated in two stages. T1: Suitable for pushing into the vertebral body with a vertebroplasty injection needle after mixing cement. T2: Suitable for pushing with a 1ml syringe after mixing. The 12-gauge vertebroplasty injection needle (Osteo Cement Needle, JMT Co., Yangju, South Korea) was inserted under fluoroscopic control through the pedicle base into the vertebral body. Manually mix the cement using conventional cement mixing equipment, checked the handling time, and transferred it into the 1 ml syringes. Each type of bone cement was injected and terminated when the adequate filling of the vertebral body was achieved or if leakage occurred following the needle was then removed (**Figure 2**). All operations were performed by an experienced senior spine

surgeon.

2.1.4.3 Cement distribution in lumbar vertebrae

The Quantum GX2 micro-CT imaging system (PerkinElmer, Hopkinton, MA, USA) was used to visualize the differences in contrast between the cement distribution and the surrounding bone.

2.1.5 In vivo study

2.1.5.1 Rabbit ilium bone defect model and surgical procedure

The animal research was approved by the International Animal Care and Use Committee (SMG-SNU Boramae Medical Center, IACUC No.2021-0006). 16 New-Zealand white male rabbits (JA BIO, Suwon, Korea) with an average weight of 3.75 kg (3.5-4.0kg) were used after an acclimation period of seven days in a conventional environment with a controlled condition of temperature(22±5℃), humidity(50±5%), and alternating 12h dark and light cycles. Care was taken to avoid unnecessary stress and discomfort to the animal throughout the experimental period. The test implants were designed as in our previous study[24]. The 7 mm long cylindrical bar with a diameter of 6 mm was connected to a 5 mm cylindrical bar with a diameter of 4mm. The thinner bar was inserted into the ilium and the thicker bar (φ:6 mm) was made to contact the surface of the ilium. The thicker bar contained a hole (φ:2 mm), which was used for wire insertion during tensile strength testing (**Figure 3**).

The surgical procedures were performed on both sides of the ilium under general anesthesia with 20mg/kg zoletil (VIRBAC S.A., Carros, France) and 10mg/kg xylazine (Bayer Korea Co., Ansan, Korea). A fascial incision was placed along the

superior border of the ilium and subperiosteal dissection was performed beneath this incision. The two (φ:4 mm) holes were made at the center of both iliac bones and irrigated with normal saline, the implants were evenly inserted into each position which was predetermined by block randomization. After generous saline irrigation of the wound, the incisions were sutured layer by layer. The Cefazolin 100 mg/kg (Chong Kun Dang Corp., Seoul, Korea) antibiotic was injected for two days after surgery to prevent infection. Under deep anesthesia, all rabbits were sacrificed with KCL (Sodium Chloride-40 Inj. Daihan, Korea) after 4 and 8 weeks. The specimens were harvested and fixed in 10% formalin. All specimens were performed Micro-CT analysis, and seven of each group underwent the tensile test, and the remainder underwent histological analysis.

2.1.5.2 Micro-CT evaluation.

The specimens were scanned with a micro-CT scanner (Skyscan 1173, Bruker, Belgium) with 130 kV voltage, 60 μA current, image pixel size of 24.94 μm, and a 1.0 mm AI filter. NRecon (Bruker, Belgium, V1.7.04) was used to reconstruct the image, and Data viewer (V1.5.1.2, SkyScan, Bruker, Belgium) was used to extract the coronal implant image and differentiated the implant from the surrounding bone tissue with color. The percentage of the length of direct bone-to-implant contact relative to the total implant surface was measured in embedded bilateral coronal implants. For each sample, five slides were randomly selected from the middle of the implant and measured, and averaged by Image J software. The quality of the cancellous bone near the implant (2 mm) was analyzed by calculating the percent

bone volume (bone volume/total volume, BV/TV), bone mineral density(BMD).

2.1.5.3 Biomechanical test (Tensile test)

The iliac bones were collected for tensile testing after 4 and 8 weeks of implantation using the universal testing machine (UTM) (TEST ONE, Loadrane: 200/100/50/20 kgf, Column type: single, Korea). A stainless steel wire was coiled around the ilium and then inserted through the hole in an implant and adjusted such that it was perpendicular to the longitudinal axis of the implant. The crosshead speed range was set at 5 mm/min.

2.1.5.4 Histological evaluation

The 10% formalin-fixed specimens were dehydrated with 70-100% ethyl alcohol and then embedded with the Technovit 7200 VLC (Kulzer GmbH Division Technik Philipp-Reis-Str. 8/13 61273 Wehrheim Germany) resin. Using a polymerization system (EXAKT, Germany) to solidify the specimens, the blocks were sectioned to a thickness of 350 μm. Then using the EXAKT grinding machine (EXAKT, Germany), the slices were ground to (40-70) μm thickness. The slices were stained with hematoxylin and eosin staining (H&E staining) and Goldner trichrome staining and then evaluated using the 3DHISTECH software CaseViewer (Budapest, Hungary) after being digitally scanned.

Part 2. Antioxidant-coated multifunctional whitlockite scaffold

2.2.1 Systemic review and network meta-analysis

2.2.1.1 Search strategy and selection of studies

It was conducted following the Preferred Reporting Items for Systemic Reviews and Meta-analyses for Network Meta-analysis (PRISMA-NMA) reporting guidelines[25]. This protocol was registered in PROSPERO with registration No. CRD42020214489. Ovid Medline, EMBASE, Web of Science, and Cochrane Library databases were searched to collect all published evidence from inception up to and including Oct 30, 2020. The search terms included extensive controlled vocabulary in various combinations, supplemented by keywords such as 'Femur Head', 'Joints', 'Osteonecrosis', 'Necrosis', and 'Orthopedic Procedures'. The search strategy used in Medline through OVID was presented in Table 2. In addition, reference reports of previous systematic reviews, meta-analyses, and randomized controlled trials (RCTs) were manually reviewed.

The PICO information was as follows: patients(P): the patients who were diagnosed as ONFH and more than 18 years of age; intervention(I): various joint-preserving procedures including non-vascular or vascular bone graft, tantalum implantation, cell-therapy (CT) including Mesenchymal stem cells, bone marrow aspirate concentrate, bone marrow mononuclear cells, et al and non-surgical or physiotherapy treatment; Comparison(C): different types of treatment as a direct or indirect comparison; Outcome measures(O): the primary outcome was the rate of conversion to total hip replacement arthroplasty (THA); the rate of radiographic progressions to next stage; the secondary outcome was HHS (Harris Hip Score) to

assess functional recovery; The study design (SD): RCT. The language was limited to English. The exclusion criteria were as follows: (1) non-RCT, laboratory scientific, or other non-relevant studies; (2) the study shared the same data set; (3) the study combined drug therapy effect with interventions or osteotomy. (4) the study focused on undesired outcomes or interventions. (5) literature report could not be extracted or converted into valid data.

2.2.1.2 Data extraction and Outcome assessment

The following information was extracted independently: the first author; publication year; sample size; the number of hips; type of intervention; sex ratio; age; stage (ARCO or Ficat or Steinberg); risk factors and follow-up time. All treatments using cell extraction in ONFH treatment were classified as cell therapy (CT) owing to no uniform standard for cell extraction and classified vascular and avascular bone grafts as VBG and BG according to whether vessels were used to supply blood. And non-surgical treatment includes a variety of physical and rehabilitation training such as physical shockwave therapy. For the part of risk factors and stage 3 considering that may be a potential interference factor and affect the results were also extracted and analyzed to reduce or evaluate possible sources of heterogeneity. Clinical primary outcomes contain the number of conversions to THA and radiographic progression to the next stage. The secondary outcome of interest was the HHS to assess clinic function (pain, joint activity, absence of deformity, and range of motion). The maximum score is 100 and higher indicates a better treatment result. Because the postoperative follow-up time was different, all the data results were based on the last follow-up reported outcomes of each study.

2.2.1.3 Risk of bias assessment and data analysis

The Cochrane Collaboration' s risk of bias tool[26] was used to assess bias according to Review Manager (version 5.3). The disagreements were resolved by the third reviewer and the methodology for each study was graded as 'high', 'low', or 'unclear' reflecting the risk of bias.

A multiple treatment comparison NMA was performed under a frequentist framework using a random-effects model. The network and mvmeta packages in Stata statistical software version 14.0 MP (State Corp)[27,28] were used to analyze the data. The network plots were used to summarize the geometry of the evidence network indicating the type of various interventions, the number of patients, and the amount of pair-wise comparison. The consistency of the network was checked with local and global inconsistency tests. Each closed loop in the network was assessed to confirm local inconsistency between direct and indirect effect estimates and only triangular (formed by three treatments all compared with one another) loops were considered.

The summary of mean differences and 95% confidence intervals (Cis) together with their predictive intervals (PrIs) were presented between comparisons. PrIs provide an interval within which the estimate of a future study is expected to be. The surface under the cumulative ranking curve (SUCRA) is a relative ranking measure that accounts both for the location and the variance of all relative treatment effects[29]. A lower SUCRA value was regarded as a better result for the primary outcome and a higher SUCRA value was regarded as a better result for the secondary outcome. A comparison-adjusted funnel plot was used to assess the presence of small-study

effects[30].

2.2.2 Antioxidant-coated multifunctional whitlockite scaffold

2.2.2.1 Material preparation and scaffold fabrication

Hyaluronic acid 0.5wt% (HA, 1.01-1.8Mda, Lifecore biomedical) was mixed in PBS, and vortexing is performed. After dissolving, whitlockite was put into the solution and sonication proceeded for 30min in ice to disperse whitlockite completely. Then, Collagen powder 0.5wt% (Cologenesis, India) was mixed in solution and obtain a uniform solution with sonication. Add EDC/NHS solution of the final concentration of 50mM/25mM, put the solution in the desired shape of the mold, and crosslinked it at -20℃ for 72hrs. The crosslinked scaffolds were freeze-dried and sterilization processes were performed to use. And the synthesis of tyramine-conjugated hyaluronic acid, tyrosinase immobilization, and dip coating of scaffold for HA_CQ conjugation were described in **Figure 4A, 4B**.

2.2.2.2 SEM and X-ray photoelectron spectroscopy (XPS)

Scaffolds were attached on specimen mount and sputter coated with platinum. The microstructure images were captured by scanning electron microscopy (FE-SEM, JSM-7800F Prime, JEOL Ltd, Japan). Additionally, scaffold surface elements were examined using energy dispersive spectroscopy (EDS). The pore size of the scaffold was calculated by measuring the length of the pore's cross section that appeared in SEM images using Image J software.

X-ray photoelectron spectroscopy was performed to evaluate the chemical structures of the scaffolds and the coated scaffolds. The scaffold was compressed by pressing the scaffold for 10 seconds at 8 ton through a pelletizer. The compressed

scaffolds were completely dried under vacuum at 50 ℃. in a vacuum oven overnight.

After that, the chemical structure was evaluated using Electron Spectroscopy for Chemical Analysis (ESCA) equipment. The carbon binding energy peak was corrected to 284.6 eV, the BG type was processed with Shirley and the line shape was processed with GL (30) through Casa XPS software.

2.2.2.3 Ion release measurement and mechanical testing

Scaffolds were prepared in sizes of Ø=4mm, and H=8mm. Each scaffold was immersed in 10 mL of DI water. The solution sample was collected after 1 day, 4 days, 7 days, and 14 days and changed to fresh DI water. The collected solution was measured using an Inductively coupled plasma atomic emission spectrometer (ICPS-8100, Shimadzu).

The mechanical strength of the scaffolds was measured by a universal test machine (Shimadzu, Japan). Each scaffold sample was located on the sample plate. The measurement was started by pressing the scaffold with 0.1 mm/s of stroke speed and the measurement stopped at strain 33.3%.

2.2.2.4 Hemolysis assay

Human whole blood, Na citrate (Innovative Research, USA) was purchased. For blood coagulation, 25 mM solution of CaCl2 was mixed with blood in a ratio of 1:2. Mixed blood solutions were immediately applied to the scaffold and tested after 5 minutes. Hemolysis and plasma release tests were performed by putting the scaffold (Ø=4mm, h=4mm) in 1 ml of PBS. In addition, the 540nm absorbance of the emitted plasma was measured through a microplate reader (Tecan, Infinite 200).

2.2.3 In vitro study

2.2.3.1 Cell viability and proliferation test

Human bone marrow stem cells (hBMSC, ATCC, PCS-500-012) were used for viability and proliferation test. Cells were seeded on Transwell plate (Corning, 3422) 7500cells/cm^2 of density with growth media. Each scaffold was placed on the insert of Transwell for 3days. For the cell viability test, cells were stained with Calcein AM/Ethidium homodimer-1 solution. Live green and dead red fluorescence cells were imaged. For the cell proliferation test, every 24hrs, Prestoblue (Invitrogen) solution was treated to culture plate with the manufacturer's guidance. Relative fluorescence intensity was used to calculate the cell proliferation ratio, as a day 0 control intensity was set to 1.

2.2.3.2 In vitro osteogenic differentiation test

hBMSCs were cultured in osteogenic differentiation medium that contains Ascorbic acid-2-phosphate (50uM, A2P, Sigma), Glycerol-2-phosphate (10mM, G2P, Sigma) and Dexamethasone (100nM, Sigma), FBS (10%v/v) in alpha-MEM. On days 7 and 21, Cells were fixed in paraformaldehyde 4% solution for 15min and washed twice with PBS. Alkaline phosphatase staining was conducted using Naphthol AS-MX (Sigma) reagent. And Alizarin red S 2% (Sigma) solution was used to detect mineralized compounds.

2.2.3.3 Reactive Oxygen species (ROS) scavenging analysis

For the ROS test, mouse bone marrow macrophage (BMM) was used. Cells were harvested from Balb/c 8weeks old mice's bone marrow. Harvested bone marrow cells were seeded with M-CSF 10ng/ml for 7 days. The attached cells were used in

further experiments as M0 macrophages. The ROS scavenging effect of scaffolds is analyzed using the H2DCFDA method. First, BMM cells are seeded on 24-Transwell plate with Lipopolysaccharide (from E.coli, Sigma) 100ng/ml. 24hrs later, cells were treated with 1uM of H2DCFDA, and each scaffold was put on Transwell. After 20min, the media was removed and cells were washed with PBS. And fluorescence intensity was determined using a microplate reader.

2.2.3.4 Real-time PCR assay

Cultured cells were harvested with TRIZOL(Thermofisher) reagent to extract total RNA with the manufacturer's guidance. cDNA was synthesized using M-MLV cDNA synthesis kit (Enzynomics, Korea). To evaluate the gene expression of differentiated cells, real-time PCR was carried out with synthesized cDNA using TOPreal SYBR green premix (Enzynomics) and StepOne Real-time PCR System (Thermofisher).

2.2.4 In vivo study

2.2.4.1 Mouse peritoneal transplantation

Mouse tests were conducted following the guidelines for the Care and Use of Laboratory Animals by the Seoul National University. 8weeks old female Balb/c mice were prepared for peritoneal transplantation. Mice were anesthetized with 100mg/kg of alfaxan and 10mg/kg rompun mixture. Then, Scaffolds (Ø=4mm, h=3mm) were transplanted into the peritoneal cavity. After 1 day, mouses were sacrificed using CO2, and scaffolds were harvested.

2.2.4.2 Mouse femur defect model

Balb/c, 8-week-old female mice were used as the model for femur defects. A mixture of alfaxan (100 mg/kg) and rompun (10 mg/kg) was used to anesthetize

mice. Then, using a drill on the femur, 4 holes with a diameter of 0.8mm were produced. The hole was filled with each scaffold (h=1mm, Ø=0.8mm) before being sutured. A mouse was sacrificed and its femur was collected 1 or 4 weeks later.

2.2.4.3 Establishment of steroid-induced ONFH in rabbits

The animal research was approved by the Institutional Animal Care and Use Committee of the Seoul Metropolitan Government Seoul National University Boramae Medical Center (SMG-SNU Boramae Medical Center, IACUC NO.2021-0013). 17 New-Zealand white male rabbits (JA BIO, Suwon, Korea) with a body weight of 3.0-3.5kg were housed in individual cages and allowed 1-week acclimation.

The ONFH model was induced by MPS (methylprednisolone acetate, methysol Inj 500mg, Alvogen, Korea) according to a previous study[31]. Briefly, three injections of 40mg/kg body weight of MPS were given intramuscularly at a time interval of 24h. During the MPS injection, The Cefazolin 100 mg/kg (Chong Kun Dang Corp., Seoul, Korea) antibiotic was injected to prevent infection (**Figure 5A**). After six weeks, the remaining 16 rabbits (one rabbit died of infection) were randomly divided into four groups: 1. Disease control group; 2. CD group; 3. WH group; 4. WH_CQ group.

2.2.4.4 Core decompression and scaffold implantation

Rabbits were anesthetized with 20mg/kg Zoletil (VIRBAC S.A., Carros, France) and 10mg/kg xylazine (Bayer Korea Co., Ansan, Korea). After a 2 cm skin incision was made over the proximal lateral thigh on both sides, CD was performed by creating a bone tunnel (approximately 27 mm) from the greater trochanter to the femoral head, using a 3 mm diameter drill bit under C-am of an X-ray machine. And different implants were transplanted into the femoral head through the bone tunnel (**Figure**

5B, 5C). Finally, the incision was closed layer by layer. The Cefazolin 100 mg/kg (Chong Kun Dang Corp., Seoul, Korea) antibiotic was injected to prevent infection before surgery and two days after surgery.

Rabbits were kept in cages and allowed free activities. At 8 weeks postoperatively, rabbits were euthanized using KCL under deep anesthesia. In the disease control group, rabbits did not receive any treatment after ONFH was established and were euthanized at 14 weeks after MPS injection. All the specimens were harvested and immediately fixed in 10% formalin for histopathology and immunohistochemistry examinations and micro-computed tomography(micro-CT) evaluation.

2.2.4.5 Micro-CT evaluation

The proximal femurs were scanned with the Micro-CT scanner (SkyScan 1173, Bruker, Belgium). The scanner settings were 13.52μm image pixel size, 59KV source energy, 0.5 mm AI filter, 167μA source current, and the 0.4°rotation step. NRecon (Bruker, Belgium, V1.7.04) and Micro-CT software (CT Analyser V1.17.7.2+, SkyScan, Bruker, Belgium) were used for all analyses. The region of interest (ROI) was defined as two parts, inside and outside areas. Inside was defined as a 3mm diameter and 2.5mm long cylindrical area located within the CD area, while outside was defined as a 2mm area ((φ5-φ3) diameter and 2.5mm long cylindrical area around the bone tunnel. And bone parameters such as calculating BMD and BV/TV. A threshold value of bony tissue was determined by a phantom.

2.2.4.6 Histological evaluation-empty lacunae

The specimens (femoral heads) were fixed with 10% formalin and decalcified with

0.5M ethylene-diaminete-traacetic acid (EDTA) at PH 7.4. The segments were embedded with the Technovit 7200 (EXAKT, Germany) resin, and then using the EXAKT grinding machine (EXAKT, Germany), a 4-μm-thick longitudinal frozen section parallel to the direction of the femoral neck axis was obtained. The prepared slides were stained with hematoxylin and eosin (H&E) staining and evaluated using the 3DHISTECH software CaseViewer (Budapest, Hungary) after being digitally scanned. Histologically, osteocytes were divided into three categories: alive, dying, and dead[32]. Outside the ROI region of the femoral head, 5 regions were randomly selected, and 100 lacunae were counted in each region under high-power fields at x200 magnification and each kind of cell was counted to determine the percentage using Image J. In the disease control group, the ROI was defined as the center region of the femoral head with an area of 3 x 4mm, assumed to be the CD region.

2.2.4.7 Immunohistochemical evaluation

Femoral head sections were immunostained for osteocalcin (OCN), tartrate-resistant acid phosphatase (TRAP), CD31 (Platelet Endothelial Cell Adhesion Molecule-one; PECAM-1), MOMA-2 (Abcam, ab33451) and TNF-α (Santacruz, sc-12744) respectively to assess effects on osteogenesis, osteoclastogenesis, angiogenesis, and inflammatory response. Immunohistochemistry was performed with anti-osteocalcin (OCN; MA1-20786, monoclonal, 1:100, Thermo Scientific Pierce Antibodies, Rockford, IL) for OCN staining, TRAP histochemical staining kit (Acid Phosphatase Kit 387-A; Sigma-Aldrich, St. Louis, MO) for TRAP staining, CD31 primary antibody (NB600-562, Novus Biologicals, Littleton, CO, USA) and

DAKO immunohistochemistry kit (GBI Labs, WA, USA) for CD31 staining, and carried out according to the manufacturer's instructions.

To evaluate the area inside and outside of the CD, five fields were randomly selected and photographed under 20× magnification (TRAP and CD31 staining) and under 40× magnification (OCN staining). The percentage of TRAP-positive staining area, the number of OCN-positive cells, and the number of CD31-positive stained microvessels were semi-quantitatively evaluated in each field with Image J. The single endothelial cell or cluster of endothelial cells clearly separated from adjacent microvessels was considered one countable microvessel.

2.3 Statistical analysis

All data were expressed as mean ± standard deviation (SD). Statistical analysis of the parametric data was performed using a one-way analysis of variance (ANOVA) with Tukey's and Dunnett multiple comparisons tests. The statistical analysis of the nonparametric data was performed using Kruskal-Wallis tests with Dunn's multiple comparison tests. All plotting of data and statistical analyses were performed using GraphPad Prism 8.1 (GraphPad Software, La Jolla, CA, USA). $P<0.05$ was considered statistically significant. Data indicated with P-value as ns (not significant), * ($p < 0.05$), ** ($p < 0.01$), *** ($p < 0.001$).

A multiple treatment comparison NMA was performed under a frequentist framework using a random-effects model. The network and mvmeta packages in Stata statistical software version 14.0 MP (State Corp)[27,28] was used to analyze the data. The

network plots were used to summarize the geometry of the evidence network indicating the type of various interventions, the number of patients, and the amount of pair-wise comparison. The consistency of the network was checked with local and global inconsistency tests. Each closed loop in the network was assessed to confirm local inconsistency between direct and indirect effect estimates and only triangular (formed by three treatments all compared with one another) loops were considered.

Chapter 3. Results

Part 1. WH-incorporated functional bone cement

3.1.1 Bone cement characteristic

The TTCP/WH bone cement showed good stability when injected into PBS solution (**Figure 6A**) and a representative surface structure of the bone cement can be observed according to SEM images (**Figure 6B**). In the EDS image of the PMMA and TTCP groups, the elements on the surface are not uniformly distributed. In particular, the TTCP group has a region where carbon elements are clustered in a spherical shape. This region shows a non-homogenous region in which calcium is hardly found. But, TTCP/WH cement has a uniform surface element distribution structure, and Magnesium which is the feature of whitlockite was measured (**Figure 6C**).

The processing temperature change over time and the setting time over mechanical strength were measured. An exothermic setting reaction occurs through the polymerization of monomers and changes cement to a rigid form, where the temperature rises rapidly (**Figure 6D**), which is consistent with the trend of setting time measured through surface compressive strength (**Figure 6D, 6E**). PMMA cement showed an injectable time of more than 15 minutes but showed the highest setting temperature of about 82℃. However, in TTCP/WH group, the maximum temperature is about 54℃, and the processing time is similar to that of PMMA cement (**Figure 6D, 6E**). The processing time was divided into 4 segments by measuring the surface physical strength of cement during setting. Each section has one minute of fixed mixing time, waiting time (1~5N), injectable time (5~100N), and setting time

(above 100N) (Figure 6F).

TTCP and TTCP/WH cement have neutral pH, the cement containing calcium phosphate neutralizes acid and reduces the acidity of PMMA cement (Figure 6G). After setting, the physical stiffness of the cement was measured and shown graphically (Figure 6H). The PMMA group shows the highest Young's modulus and HEMA lower cement's Young's modulus significantly compared to the PMMA group. The other two groups have higher Young's modulus than HEMA but, decreased in comparison with PMMA (Figure 6I left). PMMA group has a yield strength 105MPa at the largest strain point and the other groups showed yield strength above 70MPa (HEMA=81.6MPa, TTCP=79.2MPa, TTCP/WH=83.5MPa), thus all groups exceeded the ISO 5833 standard of mechanical compressive strength-70MPa (Figure 6I right). The measurement of bending strength through the 3-point bending test confirmed that the HEMA group showed the highest level, and the calcium phosphate added groups showed a slightly lowered value when compared to the PMMA group (Figure 6J).

3.1.2 In vitro study results

3.1.2.1 Osteogenic and anti-adipogenic effect of TTCP/WH bone cement

The effect of cement on cell proliferation, survival, and differentiation was investigated through in vitro experiments. All experiments in Figure 7 were performed with human bone marrow mesenchymal stem cells(hBMSC), and scaffolds of diameter=5mm and height=4mm were added to the cell media at a concentration of 0.1 g/ml for each cement group, and this conditioned media used for cell culture.

The viability of cells was unaffected by any of the cement-conditioned mediums. Cell death was not seen after 24-hour cell culture, as shown by Calcein/EtBr staining (Figure 7A). Absorbances were measured using a prestoblue-cell viability assay, and the relative intensity was described by date. In the case of the HEMA group, cell proliferation was lower than that of the control group, but it was not statistically significant, and other groups did not affect the degree of cell division (Figure 7B). Both TTCP and TTCP/WH groups containing calcium phosphate can affect cell differentiation through the release of Ca, Mg cations. The kinetics of ion release from the surface of cement were monitored. For 21 days, Ca ions were measured in the TTCP group and Ca and Mg in the TTCP/WH group. The TTCP/WH group showed a lower amount of calcium release (34.2ppm) than the TTCP group (42.1ppm), but the total cation release (45ppm) showed a higher amount of release than that of TTCP (Figure 7C). We investigated how substances released from cement affect the genes and differentiation of cells. hBMSCs cultured on cement-conditioned growth media were genetically analyzed by RT-PCR on days 7, 14, and 21. The PMMA and HEMA group condition media increased the gene of Adiponectin, which is characteristic of adipogenesis, and the TTCP, TTCP/WH group increased RUNX2, a gene related to bone differentiation. Then, hBMSCs were cultured through osteogenic-cement-conditioned media and adipogenic-conditioned media. And the degree of differentiation and gene expression changes were analyzed. ALP staining on day 7 of osteogenesis and the ARS on day 21 was the highest in the TTCP/WH group, indicating osteoconductive property and assisting mineralization of whitlockite (Figure 7D). Also, bone differentiation-related genes ALP, RUNX2, and COL1 were

measured the highest in the TTCP/WH group, whereas the HEMA group had the lowest level of gene expression (**Figure 7E**). Oil red O Staining was performed to identify adipogenic differentiated cells (**Figure 7F**). Compared to the control group, the calcium phosphate group could hardly detect fat staining with oil red. And, when examining the expression of fat-related genes, PPAR-gamma, CEBPa, and Adiponectin, it can be confirmed that the PMMA group is enhanced but, calcium phosphate significantly lowers the fat lineage-related gene expression. (**Figure 7G**).

3.1.2.2 Focal adhesion of hBMSCs on bone cement scaffolds

PMMA cement is bio-inert and has hydrophobic properties. Because of this, cells are difficult to adhere to cement surfaces, which increases the chance of fibrosis and this can induce necrosis. Therefore, the cells were attached directly to the cement scaffold, and the focal adhesion conditions were observed. First, cells were seeded directly onto thin, flat cement scaffolds. 24 hours after cell seeding, cell adhesion, and viability were confirmed through Calcein AM/EtBr staining (**Figure 8A**). The fluorescent image demonstrated the PMMA cement surface's unfriendly structure for cell attachment. Most of the cells were alive, but due to their inability to extend their feet, cells did not adhere to the PMMA cement and have spherical in shape. Also, most of the cells died on the surface of HEMA cement. This is presumed to be due to the strong acidity of the HEMA surface. Most of the cells in the TTCP and TTCP/WH groups were alive, and the feet of the cells were well extended (**Figure 8A, 8B**). Thereafter, the surface was harshly washed several times with a pipette, the cells were fixed, and the cells that remained on the surface of the cement were observed by staining with phalloidin (**Figure 8C**). After washing, no cells were found

in the PMMA cement, and most of the cells were still strongly attached to the TTCP and TTCP/WH cement surface (**Figure 8D**). Intermediate filament Vimentin and focal adhesion related Paxillin were stained with the immunofluorescence method. A clear difference in focal adhesion was identified between PMMA and TTCP/WH cement groups. On PMMA cement, most cells do not maintain their original form, but on WH cement, in the enlarged image, Paxillin mediates focal adhesion with the cement surface and maintains its shape to function normally (**Figure 8E, 8F**). hBMSCs were attached to the cement surface, cultured in osteogenic media for 1 week, and osteogenic differentiation was measured through ALP staining. In the PMMA and HEMA groups, it was observed that the number of cells stained with ALP occupies only a small area. In the TTCP and TTCP/WH groups, ALP measured area was significantly enhanced, and TTCP/WH group showed a more stained region of bone differentiation relative to phosphatase of hBMSC than the TTCP group (**Figure 8G, 8H**).

3.1.3 In ex-vivo study results

In operational working times, there was no difference between TTCP/WH group and the pure PMMA group which was longer than TTCP (**Figure 9A**). And there was also no significant difference in the distribution of bone cement in the vertebral body. Its distribution characteristics were shown in **Figure 9B.**

3.1.4 In vivo study results

3.1.4.1 Micro-CT results

The representative micro-CT images of the two different planes (coronal and transverse) were shown in **Figure 10A**. Bone-to-implant contact images were

observed with Data viewer tools and analyzed the contact ratio. Compared with the PMMA group, tight bone bonding was observed between bone and the cement and the bone–implant contact ratio significantly increased in TTCP and TTCP/WH groups at 4 and 8 weeks (**Figure 10B**). And there was a statistical difference at 8 weeks (P=0.0322 and P=0.0112, respectively). For the bone parameters of the ROI area around the implant, the BMD and percent of BV in the TTCP group and TTCP/WH group showed higher levels than in the PMMA group, and its more obvious in the TTCP/WH group. At 4 weeks, new bone formation was observed around the implants, there were statistical differences in BMD compare with the PMMA group (P = 0.0147 and 0.005). By the 8 weeks, both the TTCP group and TTCP/WH group increased BMD and showed better bone regeneration around the implant with the statistical difference in BV/TV(P = 0.0476 and P < 0.0001 vs PMMA). In addition, in the 8th week, it also showed a statistical difference between the TTCP group and TTCP/WH group in BMD and BV/TV(P = 0.0383 and P = 0.0494), that is, the addition of WH further improved its osteoconduction and promoted bone regeneration. (**Figure 10C**).

3.1.4.2 Biomechanical Test (Tensile strength)

The biomechanical testing system was shown in **Figure 11** to illustrate the bone and cement fusion strength. The results of tensile strengths in experimental groups (TTCP and TTCP/WH) showed higher levels at 4 and 8 weeks, it was more obvious and showed statistical differences at 8 weeks (P=0.002 and P=0.0009) compared to the PMMA group. Despite there being no statistical differences between TTCP and TTCP/WH groups.

3.1.4.3 Histological results

The representative histological H&E and Goldner's trichrome staining images after implantation at 4 and 8 weeks were shown in **Figure 12**. The inserted cylinder was tightly connected to the ilium, and new bone tissue formation was observed around the TTCP and TTCP/WH. The thickness and length of the new bone formed along the implant were thicker and longer than the PMMA group. In addition, relatively massive new bone formation was also observed around the implant in the unembedded ilium (**Figure 11B**), the contact surfaces between the bone and the implant can also be observed, and it's larger than those of group PMMA and HEMA groups. Especially, when Goldner's trichrome staining was performed, the phenomenon of new bone formation was clear (**Figure 12**).

Part 2. Antioxidant-coated multifunctional whitlockite scaffold

3.2.1 Network meta-analysis of ONFH

3.2.1.1 Characteristics of included studies and risk of bias

A PRISMA diagram summarizes the literature search results and study selection for this systemic review and NMA is shown in **Figure 13**. Of the 7896 citations identified through our literature search (1702 after duplicates were removed), 6162 were deemed ineligible after the title and abstract screening, leaving 32 to articles search for full-text review. In total, 17 RCTs[20,33-48] involving 784 patients (918 hips) met the inclusion criteria and were accepted. Including Non-surgical treatment, CD, CD+bone graft (BG), CD+TI (tantalum rod implantation), CD+Cell therapy (CT), CD+BG+CT, and vascularized bone graft (VBG). The basic characteristics of the included studies are summarized in **Table 3.**

The risk of bias of the included studies in this NMA was generally unclear or high. Overall, studies fulfilled the criteria for a judgment of a high risk of bias. Details about the risk of bias assessment were graphically summarized in **Figure 14**. The study was deemed high risk.

3.2.1.2 Results of network meta-analysis.

Figure 15A, 15B showed the network plot of the risk factors induced to ONFH and the proportion of stage 3 in each intervention, respectively. And the results showed that there was no significant statistical difference between each intervention in **Figure 16**.

3.2.1.3 Radiographic progression

Figure 14C depicted the network plot of the various JPT methods comparing the rate

of radiographic progression results. seven interventions (CD, CD+BG, CD+TI, CD+CT, VBG, and Non-surgical treatment) were compared in 15 studies[20,33-36,38-44,46-48] and pooled results. CD and CD+CT were compared directly more than the other treatment. CD and CD+CT was the most frequent comparator in our studies. Three comparisons (CD+BG vs CD+BG+CT, CD+BG vs VBG, and CD vs CD+CT) were conducted using direct evidence alone. Five comparisons were performed using mixed evidence (both direct and indirect evidence) and 13 comparisons using indirect evidence alone.

There were two closed loops and no significance in the local inconsistency between the direct and indirect point estimates (**Figure 15F**), and no network inconsistency [χ^2 (2)=1.87, p=0.392]. CD+CT showed a statistical difference and relatively superior result than non-surgical treatment, CD, and CD+BG, which were significant only in 95% Cis but not in 95% PrIs (**Figure 17A**) which means that any future RCT could change the significance of the efficacy of these comparisons.

The cumulative ranking plot was drawn, and the SUCRA probabilities were calculated (**Figure 18A**). According to the SUCRA value, CD+CT (96.4%) showed the relatively best result, followed by CD (64.1%), CD+BG+CT (59.2%), VBG (48.5%), CD+TI (43.3%), Non-surgical treatment (24.3%) and CD+BG (14.3%). The comparison-adjusted funnel plots showed that the funnel plots were symmetrical around the zero lines, which suggested a less likely publication bias (**Figure 19A**).

3.2.1.4 Conversion to THA

Figure 15D displayed the network graph of the seven interventions (CD, CD+BG, CD+TI, CD+CT, VBG, and Non-surgical treatment) that were compared in 15

studies[20,33-36,38-44,46-48] in terms of conversion to THA. CD and CD+CT were more studies when compared directly to the other JPT methods. Four comparisons (CD vs CT, CD+BG vs CD+TI, CD+BG vs CD+BG+CT, and CD+BG vs VBG) were conducted using direct evidence alone. Two comparisons were using mixed evidence and 15 comparisons used indirect evidence alone.

There was no available loop formed by the study arms, and loop-specific tests were not performed. No significant differences among the JPT methods in terms of both CIs and PrIs were found, other than CD+CT showed a lower rate than CD+BG only in terms of the Cis (**Figure 17B**).

The SUCRA plots (**Figure 18B**) showed that the rate of conversion to THA was lowest in CD+CT (90.4%), followed by CD (69.1%), CD+BG+CT (58%), VBG (47.6%), Non-surgical (46.2%), CD+BG (24%), and CD+TI (14.8%). The comparison-adjusted funnel plots suggested a less likely publication bias (**Figure 19B**).

3.2.1.4 Harris Hip Scores

The network plot comparing the HHS was depicted in **Figure 15E**. Six JPT methods (CD, CD+BG, CD+TI, CD+BG+CT, VBG and Non-surgical treatment) were compared in 7 studies[20,33,37,38,40,43,46]. Five comparisons were conducted using mixed evidence and 10 comparisons using indirect evidence alone. There was no available loop formed by the study arms.

There was no significant difference among these methods in CIs and PrIs other than CD+BG showed a higher score than Non-surgical treatment only in terms of Cis (**Figure 17C**). The SUCRA plot displayed that the HHS (**Figure 18C**) was the highest

in non-surgical treatment (80.5%), CD+CT (72.8%), CD+TI (54.0%), CD (48.7%), VBG (34.8%) and CD+BG (9.2%). Publication bias was less likely in the comparison-adjusted funnel plot (**Figure 19C**).

3.2.2 Antioxidant-coated whitlockite scaffold characteristic

The WH_CQ scaffold was examined by scanning electron microscope (SEM). As shown in **Figure 20A**, approximately 100μm of pore size was filled with a coating solution. The silk-like pattern on the scaffold surface demonstrates the cross-linked HA_CQ. And evenly distributed WH nanoparticles were found in the high magnification image (**Figure 20A**). The physical properties of WH and WH_CQ scaffolds were measured using a universal test machine (UTM). The coated WH_CQ scaffold (241.0 ± 32.5 kPa) showed twice the strength compared to the WH scaffold (122.7 ± 8.5 kPa) in dry conditions (**Figure 20B**). The scaffold restored its shape when rehydrated after the hydrated scaffold was squeezed out. This shape memory property would make it easy to implant the scaffold into the defect after CD.

To compare the chemical composition of the WH and WH_CQ scaffold, the carbon, oxygen, and magnesium were quantified by X-ray photoelectron spectroscopy (XPS). In both WH and WH_CQ scaffolds, the peak of Mg2p derived from whitlockite was observed. Especially, the chemical structure of the π-π* bond was observed only in the WH_CQ scaffold due to additional functional groups in the coating materials of phenol, catechol, and quinone (**Figure 20C**). For the ion release kinetics from whitlockite, WH and WH_CQ were incubated in distilled water, then filtrated, and conducted an inductively coupled plasma atomic emission spectrometer (ICP-

AES). The coating process did not change releasing of Ca, Mg, and P ions. It was expected that the coating process would not significantly affect the osteogenesis ability of whitlockite (**Figure 20D**).

The blood-contacting biomaterials should not negatively interact with blood components or cause them to be destroyed[49]. In addition, blood swelling was anticipated to provide an increase in the volume of the scaffold that would promote implant stability. The volume change and the hemolysis were investigated by swelling human blood to the scaffold. Given the same amount of blood, the control collagen group (Col) tended to slightly lose its volume. However, the WH and WH_CQ scaffolds increased their volume (**Figure 20E**), and extruding force was observed due to the increased volume (**Figure 20F**). Also, both WH and WH_CQ exhibited relatively low hemolysis after coagulation of blood (**Figure 20G**). Compared to the Negative group (Neg), the hemolysis degree was decreased in the order of Col, WH, and WH_CQ (**Figure 20H**). The same tendency was observed when the amount of plasma emitted from the scaffold into the solution every minute was measured with 540 nm absorbance (**Figure 20I**).

3.2.3 Inflammation modulatory effect of WH_CQ scaffold

Antioxidant effects through ROS scavenging of the catechol quinone moiety have been investigated in several studies[50,51]. In vitro and in vivo experiments were conducted to confirm ROS modulatory effect. Each scaffold was implanted into the mouse's peritoneal cavity. After 24 hours, the scaffold was harvested and the cell layer formed around the scaffold surface was observed. Histological pictures of the scaffold surface were exhibited, and these images showed increased recruitment of

monocyte and macrophage (MOMA) in the WH group compared to the Col group, while significantly decreased in the WH_CQ group (**Figure 21A, 21B**). The H2DCFDA assay was further conducted to evaluation ROS scavenging effect of the scaffold. The amount of ROS produced in the bone marrow macrophages was quantitatively measured through the fluorescence intensity of the H2DCFDA reagent. The fluorescence intensity was the lowest in the WH_CQ group, and the WH group showed higher intensity than the Col group (**Figure 21C, 21D**). The expression of pro-inflammatory-related genes was investigated. Interestingly, the expression level of IL-1β and TNF-α were significantly decreased in the WH_CQ group (**Figure 21E**). 1mm of four defects were made in the mouse femur, and four groups Neg, Col, WH, and WH_CQ were applied to the defects (**Figure 31F**). TNF-α immunostaining was performed on the harvested femur bones after 1 week. In the WH scaffold, TNF-α staining was identified along the surface of the scaffold (red arrows), suggesting that this immune response of the scaffold upon implantation can form fibrous tissue on the implant-tissue interface. On the other hand, in the WH_CQ group, TNF-α staining was confirmed only inside the scaffold, showing a different pattern from that of the WH group (**Figure 21G**). To our best knowledge, ROS-controllable scaffold for post-CD therapy was reported for the first time.

3.2.4 In vitro study results

3.2.4.1 hBMSCs viability and proliferation

Through in vitro research, the effect of scaffolds on cell proliferation, survival, and differentiation was studied. First, we investigated whether the scaffold affects cell

viability and proliferation. In each group, scaffolds were provided to hBMSCs cells through indirect contact using transwells. The scaffold did not affect cell viability at all, which can be seen in the Calcein AM/Ethd staining image with no red-stained dead cells (**Figure 22A**). In addition, the reducing ability of cells to quantitatively measure cell proliferation for 5 days. The scaffold didn't change cell proliferation capacity significantly (**Figure 22B**).

3.2.4.2 Osteogenic differentiation and real-time PCR assay

WH in the scaffold can introduce osteogenic differentiation of stem cells through the release of calcium, magnesium, and phosphate ions[13]. To discover the osteogenic potential of the scaffolds, we investigated cell behaviors and in vivo tests. hBMSCs were cultured with scaffold and osteogenic media. The WH and WH_CQ groups had higher levels of differentiation which were investigated in alkaline phosphatase staining on day 7 and Alizarin Red S on day 21, showing osteoconductive properties that helped the mineralization of stem cells(**Figure 22C**). Additionally, the whitlockite incorporated groups retained the significantly increased levels of osteogenic differentiation-related genes ALP, RUNX2, and COL1, whereas Col group detected the lower levels of gene expression (**Figure 22D**).

3.2.4 In vivo study results

3.2.4.1 Micro-CT results

The representative micro-CT reconstruction image of the proximal femur and ROI areas was shown in **Figure 23A**. The obvious new bone formation was found inside the ROI in the scaffold implanted group than simple CD. BMD and BV/TV inside the ROI showed higher levels and had significant differences between the CD group and

scaffold groups($P<.05$). And although the bone parameters in the CD group had not yet reached the disease control level, it was found in a scaffold that their values had basically reached the disease control level and even tended to be higher. In addition, obvious changes were also found in the outside area. There was obvious enhancement along the boundary of the bone tunnel compared with the disease control group in the CT images. Significant statistical differences were also shown in the bone parameters (BMD and BV/TV), which increased significantly in the scaffold group. In the CD group, although the same phenomenon was also found, its value increased but no statistical difference was found. And the differences in bone parameters between WH and WH_CQ were small (**Figure 23B, 23C, 23D**).

3.2.4.2 Histological analysis of osteocytes

The representative photomicrographs of H&E staining and different morphological classifications of osteocytes are shown in **Figure 24**. Although there were no significant differences in the percentage of living osteocytes (normal osteocytes) between the groups (the disease control group vs the CD group vs CD+WH vs CD+WH_CQ: 53.45±1.51% vs48.68±6.2% vs 53.03±9.53% vs 50.63±8.87%), Interestingly, the percentages of the dying and dead osteocytes (pyknotic osteocytes and empty lacunae) showed some differences. Compared with the disease control group, it was found that the percentage of empty lacunae in the other groups decreased significantly, while the percentage of pyknotic osteocytes was increased with statistical significance. (the disease control group vs the CD group vs CD+WH vs CD+WH_CQ: 21.33±3.13% vs 15.05±2.56% vs 16.25±3.41% vs 15.25±2.55% in

empty lacunae; 25.48±2.73% vs 36.03±4.32% vs 30.98±8.02% vs 34.1±6.9% in pyknotic osteocytes). And there were no significant differences between CD and scaffolds at 8 weeks.

3.2.4.3 Immunohistochemical results

The representative photomicrographs of the OCN staining were shown in **Figure 25** Inside the ROI area or bone tunnel, the number of positive OCN staining cells was significantly higher in the scaffold groups than in disease control and CD groups, there was a statistical difference($p < .05$). Outside the ROI area or the area around the bone tunnel, it can still be observed that there were more OCN positive cells than the disease control group, and there was a statistical difference($p < .05$). In addition, no significant statistical difference was observed between the disease control group and the CD group, the same goes between scaffold groups.

The representative photomicrographs of the TRAP staining were shown in **Figure 26**. The TRAP staining cells were observed between the trabecular bone, and the percentage decreased compared with disease control and CD groups, although there was no statistically significant difference at 8 weeks inside and outside of the ROI areas.

The representative photomicrographs of the CD31 staining were shown in **Figure 27**. The number of CD31-positive stained micro-vessels both inside and outside the ROIs was significantly higher in scaffold groups than in the disease control and CD groups, and there were statistical differences ($p < .05$), which was more obvious in the bone tunnel or inside the ROI area. In addition, although the number of CD31-positive stained micro-vessels increased in the CD group, there was no statistical

difference compared with the disease control group.

Immunofluorescence staining of TNF-α was carried out in each sample (**Figure 28**). An increased fluorescence intensity of TNF-α in the local CD legion was distinguishing compared to the disease model group. Although the fluorescence intensity of the WH implanted group tended to slightly decrease compared to the CD group, TNF-α expression was identified in the overall area. Also, a significant amount of TNF-α was stained at the tissue-scaffold contact. On the other hand, in the WH_CQ implanted group, only local TNF-α or non-fluorescence was detected in many areas. It is determined that the CQ coating has the effect of reducing the inflammation response caused by scaffold implantation.

Chapter 4. Discussion

Part 1.

1. WH-incorporated functional bone cement

PMMA bone cement is a commonly used filling material in orthopedic surgery, but its application scope is limited due to the lack of biological activity and the high elastic modulus, and cannot achieve ideal therapeutic effects, such as in the treatment of OVCF[52]. Therefore, improvements have also been attempted in previous studies, such as adding biologically active substances to PMMA cement including active nano-MgO particles, carboxymethyl chitosan, and ferrimagnetic glass-ceramic[53-55]. However, the ideal bone cement has not yet been made and used in clinical work. We applied TTCP and WH into the PMMA cement to prepare a new functional bone cement to enhance biological activity. Fabricated TTCP/WH cement was compared bio-functionality with the bioinert PMMA cement and calcium phosphate-induced characteristics were investigated.

The international standards of PMMA bone cement (ISO 5833) are an important reference for the manufacture of new bone cement. Process time, temperature, and mechanical properties are important variables in clinical application. During vertebroplasty, commercial PMMA cement has an injectable time of about 10~15 minutes before hardening begins[56]. Also, neurological impairments are reported because of the cement leakage from the improper setting of PMMA polymerization[57]. TTCP/WH cement has 15 minutes of injectable time similar to PMMA cement while presenting undissolved features in wet conditions. Accordingly, our TTCP/WH cement is regarded to be suitable for usage in practical circumstances compare to

the TTCP group which has a relatively short injectable time. And the high polymerization temperatures of PMMA bone cement may lead to serious cell death reported by Castaldini et al.[58] that cannot repair the injury site. The exothermic temperature of the TTCP/WH bone cement in this study was significantly lower than that of pure PMMA, effectively reducing the potentially harmful heat generated during the polymerization process. This is due to the optimization of the ratio of highly reactive HEMA that is added to improve mixing and non-reactive calcium phosphate. Incorporation of calcium phosphate that disturbs polymerization reduced about 30℃ of the setting temperature of PMMA cement which coincides with the change in the proportion of the PMMA occupying the total volume.

The mechanical properties and appropriate elastic modulus of cement are the most important factors to be considered, because mismatched elastic modulus between bone cement and surrounding bone can easily lead to vertebral refractures, with a reported incidence of 15-29%[59,60]. Relatively strong stiffness and strength of PMMA compared with native bone were considered key reasons leading to subsequent vertebral fracture[61,62], although the commercial PMMA bone cement can provide support for the compressed vertebra and restore the height of the fractured vertebral body and stabilize the structure. In our experiments, HEMA in polymer structure effectively decrease its Young's modulus and showed a relatively lower value than PMMA cement when applied to TTCP/WH while maintaining compressive strength above ISO standards. Furthermore, the uniformly distributed calcium phosphate of TTCP/WH cement appears to lower the stiffness of the overall structure than that

of the TTCP group. These mechanical features will effectively reduce the impact on adjacent bones, that is, avoid the risk of recurrent fractures while effectively acting as a support, when applied to osteoporotic vertebrae.

The ideal bone cement is generally considered to be easy to inject, biocompatible has osteoinductive and osteoconductive characteristics[63]. Calcium phosphates are osteoconductive material that aids in the mineralization of osteoblasts. Our previous showed that WH had better osteoconduction and bone regeneration effects than other calcium phosphates—hydroxyapatite. In the present study, In vitro tests represent Whitlockite incorporation in cement enhances the osteoconductive effect on hBMSC cells and osteogenesis—related gene expression compared to only the TTCP group. Therefore, TTCP/WH cement can strengthen surrounding bones by providing an osteoconductive effect after being injected into the vertebroplasty site. As a bioinert material, PMMA lacks biological activity. PMMA cement neither forms chemical bonds nor osseointegrates with the bone tissue at the implant site[64], resulting in the formation of an obvious interface and the weakening of the bonding strength between the bone cement and the host bone. This will inevitably cause micro—movement between the host bone and the cement, causing tiny wear debris that will lead to osteolysis, which further leads to aseptic loosening or even displacement of the cemented implant[65,66]. This often requires revision surgery. Interestingly, hBMSCs exhibited strong focal adhesion on TTCP/WH cement. Calcium phosphate provides a neutralized pH of the cement surface and promotes focal adhesion of cell surface receptors. The more homogeneous surface structure of TTCP/WH cement is considered to give stronger focal adhesion than TTCP.

The animal experiments in the ilium bone defect model showed that the osseointegration ability in the TTCP and TTCP/WH groups was significantly increased during the follow-up period compared with the PMMA group, and there was a statistically significant difference at 8 weeks. Analysis of bone parameters by Micro-CT showed that TTCP and TTCP/WH also have obvious positive effects on bone regeneration around bone cement implant, and the TTCP/WH group showed higher levels than the TTCP group, in other words, the addition of WH further improved its osteoconduction and promoted bone regeneration. The tight connection between the functional bone cement and the host bone, and the effect on the osteogenesis of the surrounding bone were further proved by histological H&E and GT staining. In addition, the biomechanical test also showed that the bonding strength between bone and cement implant of the TTCP/WH group was significantly higher than that of the PMMA group. That is, the newly synthesized functional bone cement effectively makes up for the above-mentioned defects of PMMA bone cement. In brief, functional bone cement can effectively combine with the host bone and have a positive effect on bone regeneration in the surrounding area, which not only helps to improve bone density and enhance bone structure but also can effectively prevent aseptic loosening and even displacement.

Despite our promising results, further research is still needed. For example, the establishment of an animal osteoporosis model can be applied to its vertebral body analysis to evaluate the effect on osteoblasts and osteoclasts. It is also necessary to further improve the optimized composition of new cement and explore more potential applications.

Part 2.

2.1 Efficacy of various joint-preserving procedures for ONFH

Early intervention and treatment of ONFH may be an effective way to preserve the femoral head or even complete healing which is also a realistic goal. In recent years, many studies[20,33-48] have been made and various JPT methods have been carried out, but it remains challenges and controversies about efficacy. In our NMA, there was no statistical difference in radiographic progression and conversion to THA, and also in HHS between JPT methods and non-surgical treatment, other than CD+CT showed a relatively superior result in radiographic progression.

Based on reported data in the USA, THA was still the most commonly performed procedure and the annual percentage of patients managed using a THA accounted for 89.5% between 2009 and 2015, reported by Sodhi et al.[67]. However, the success of non-replacement procedures is also critical to the patient's quality of life and the impact on the healthcare system. Many advents of new surgical procedures have been made and more effective or available treatments have also been performed before progressing to joint collapse or implementing THA treatment because it is a realistic goal to preserve femoral head and complete healing for ONFH.

Simple CD has become the reference technique widely used in patients with early-stage ONFH Since popularized by Hungerford et al.[68]. But the results of CD are always debated and controversial[47,69,70]. The efficacy of CD has been considered that it can decrease intraosseous pressure, alleviate bone marrow edema and improve blood supply for the femoral head[43,48,71]. However, other studies[72-74] questioned and reported that, in fact, CD was not superior to non-surgical treatment, it cannot repair

the femoral head which even lowers its biological strength and causes collapse. They found that when there is a subchondral fracture (47% in ARCO stage 3), compared with the pre-collapse stages (85% in ARCO stage 1 and 65% in ARCO stage 2), the success rate of CD is even worse[75,76]. Koo KH et al.[47] at their RCT study also found that CD may be effective in symptomatic relief but is of no greater value than conservative management in preventing collapse. Based on our NMA, there were no statistical differences in primary and secondary outcomes compared with other JPT methods and non-surgical treatment, although inferior to the CD+CT method in terms of radiographic progression. Owing to CD's unpredictable and different results especially in long-term results, and to improve the limitations, several other JPT methods have been proposed and improved in recent years and achieved some promising results on ONFH outcomes versus CD.

Cell therapy, especially stem cells, has been a research hotspot in recent years and is used for tissue regeneration due to its ability to differentiate into multiple cell lineages[77]. It is generally believed that mesenchymal stem cells (MSCs) can release exosomes, which contain cytokines that promote bone formation, cartilage formation, and angiogenesis, including bone morphogenetic protein 2, vascular endothelial growth factor and transforming growth factor β[78,79]. Therefore, stem cell transplantation is expected to become a new method of ONFH combined with CD. The purpose of adding MSCs to the CD tunnel is to provide osteoprogenitor cells and vascular progenitor cells in the decompressed necrotic bone area to promote tissue regeneration and repair reported by Goodman et al.[80]. Since the CD+BMSCs for

ONFH were proposed by Hernigou et al.[81] in 2006, many studies achieved promising results. Gangji et al.[44] concluded that cell implantation delayed the progression of stage 1–2 osteonecrosis and decreased hip pain and joint symptoms more effectively than CD during a sixty-month follow-up period. And meta-analysis also found that it had better pain relief, clinical outcomes and provided a significant improvement in terms of survivorship over time compared with CD alone[82,83].

However, there were also different results. Hauzer et al.[36] at a double-blind RCT compared the CD with the CD+BMAC and found that implantation of it after CD did not produce any improvement in the evolution of ONFH in stage 3. Lim et al.[84] also assessed the clinical effects and radiological results according to a controlled trail and found that CD+CT method was ineffective in stage III–IV patients and there were no statistically significant differences between CD+CT and CD+BG in success rate or the clinical and radiographic results. In our NMA, we found that there was a statistical difference and had relatively superior results than non-surgical treatment, CD, CD+BG, and VBG in radiographic progression, but not in conversion to THA and HHS. Therefore, we think that it may be an effective method for delaying disease progression or reducing disease development based on current evidence, especially in stage I and II.

Non-vascularized bone graft was also a choice for ONFH, Since Phemister[85] was one of the first authors to describe the use of non-vascularized bone graft (NVBG) from the tibia for ONFH. Multiple studies have shown the success of this support following necrotic segment decompression to allow for subchondral bone remodeling

and healing[86,87]. Deqiang et al.[38] at RCT study reported that CD+BG can relieve hip pain, and improve function with much lesser surgical trauma compared to VBG, so it is a better choice for ONFH. However, Wang C et al.[46] reported that the shock-wave conservative treatment appeared to be more effective than CD+BG in early-stage ONFH, although the mechanism remains unknown. Based on our network results and rankings results, CD+BG had no obvious advantage in terms of primary and secondary outcomes and no statistical differences.

As a good choice of mechanical substitute, the technique of porous tantalum rod implantation (TI) was applied in medical science for more than half a century[33], Because of its advantages of superior strength, fatigue properties, biocompatibility, and initial stability for bones to those of natural osseous grafts, and they have low cytotoxicity and bacterial adhesion force[88]. Hua KC et al.[89] in their meta-analysis showed that CD combined with TI showed satisfactory clinical results. However, some research argues that this method can only provide temporary structural support until new bone growth in the necrotic lesion and the absence of new bone tissue growing into porous tantalum rods in necrotic lesions made this method less ideal[90,91]. According to histopathologic search and analysis, the clinically failed implants found that among the 15 specimens, there were 14 cases of residual osteonecrosis, and all cases had subchondral fractures of the femoral head, among which 60% of the femoral head collapsed by Tanzer M et al.[91] Based on our study, CD+TI did not have a significant advantage as compared with other JPT methods in primary and secondary outcomes and no statistical difference.

VBG is also one of the popularized JPT methods for ONFH, some studies had showed

that it was a better treatment option than CD combined with non-vascularized bone graft because not only provides structural support but also restores vascular supply to enhance lesion healing[92-94]. However, high technical requirements and a relatively low success rate of surgery have to be considered. As reported, the failure rate of vascularized grafts ranged from 4% to 30%[95,96]and most of them were found in chronic steroid users as reported in the literature[97]. Meloni et al.[98] reported that vascularized fibular graft (VFG) failure appears to be related to the negative effect of creeping substitution and supports unbalanced bone resorption enhanced by corticosteroids. Although Ji Wang et al.[99] showed that VFG was the superior effect on reducing treatment failure rates in their network meta-analysis, our results were not exactly consistent with them, the effect was not so superior compared to other treatments. Although the risk factors for ONFH were not statistically different in each intervention, we found that chronic steroid-using is one of the main induce factors to ONFH and accounted for 25% (15/60) in the VBG group. This may be one of the main reasons for the difference. Reviewing the literature in our studies, VBG may be an effective treatment, but based on our results, considering various factors, VBG was not the best option treatment for ONFH especially in chronic steroid users. This network meta-analysis assessed the various JPT methods containing the conservative non-surgical treatment in patients of ONFH. Although all available JPT methods have not been evaluated and further studies are needed, our NMA provides some important information about various methods of Joint-preserving treatment and references to select appropriate JPT methods in ONFH. The data suggest that there was no statistical difference in radiographic progression and conversion to

THA, also in HHS between above the JPT methods, other than CD+CT showed a relatively superior result in radiographic progression than nonsurgical treatment, namely, it's an effective method for delaying disease progression or reducing disease development based on current evidence.

2.2 Antioxidant-coated multifunctional whitlockite scaffold

CD is a minimally invasive joint-preserving procedure commonly used for the early treatment of ONFH to relieve the symptoms of the disease and facilitate blood circulation. The rationale of the CD technique is to reduce intraosseous pressure in the femoral head, reduce pain and restore blood flow, helping the healing of necrotic debris[19,39]. However, incomplete bone regeneration in the bone tunnel has also been found after CD or restorative osteogenesis appears to be insufficient due to well-known side effects. Especially in steroid-administered patients which are associated with osteoblast death and decreased osteoblast proliferation, thereby impairing the ability to repair and replace necrotic lesions[21,100,101]. The bone ingrowth limitation can cause bone defects and increase the risk of fracture for lacking the support structures in the subchondral bone area[102]. To improve the effectiveness of CD and facilitate defect repairing and improving mechanical support, several adjunctive therapies were tested, such as bone grafting, mesenchymal cells, tantalum rod insertion and platelet-rich plasma (PRP), etc. [101,103,104]but were not optimal and further research is still needed.

WH is synthetic calcium phosphate material that has an osteoconductive effect. In our previous results, WH can upregulate osteogenic genes and helps osteoblast mineralization[13,105]. Also, releasing magnesium is a distinguishing feature of WH that

locally enhance new bone formation in the regeneration process[106], which showed better bone regenerative effect than other calcium phosphates (hydroxyapatite and tricalcium phosphate) in bone defect animal models[13,105]. In this study, we confirmed again the biological characteristics of WH, that is, upregulate osteogenic genes such as ALP, RUNX2, and COL1, Simultaneously, it can also be observed through in vivo experiments that compared with CD alone, WH can restore bone volume faster and enhance local and peripheral bone density that effectively compensates for the above-mentioned limitations after CD. In addition, it can be also observed by immunostaining that it not only has a positive effect on osteogenesis and angiogenesis but also has a certain inhibitory effect on osteoclastogenesis. For the treatment of ONFH, WH had a positive effect on delaying the progression of the disease, that is, delaying the transformation of normal osteocytes into empty lacunae. In manufacturing medical devices, strategies to pass clinical trials are important. Strategies using enzymes have the advantages of functional efficiency, substrate specificity, and relatively mild reaction conditions[107]. However, the direct mixing of enzymes into biomaterials can lead to unpredictable side effects of residual enzymes, making clinical trials more difficult. The enzyme immobilization method can solve this residual problem, also increase the reusability of enzymes, and reinforce structural stability[108,109]. We coated the surface of the bone scaffold with HA_CQ through an immobilized Tyrosinase-based reaction mechanism. Tyrosinase was attached to the glass bead, and through the dopachrome conversion method, it was confirmed that the immobilized enzyme generates the same reaction as the unattached enzyme. Moreover, no residual enzyme is present in the reacted solution even under vigorous

physical conditions. This coating method shows the enhancement of physical properties and suppression of ROS production without the risk of residual enzyme in the following experiments.

When the biomaterials are implanted into the body, foreign body reaction is a typical response in most cases[110]. And following acute and chronic inflammation recruit macrophages and other immune cells that form a fibrotic matrix at the implant site. Finally, foreign body reaction induces fibrous capsule formation around the implanted biomaterials[111]. This fibrous capsule cause malfunction of medical devices and leads to implant failure such as dislocation and loosening[112]. Therefore, strategies that contain modification of biomaterials or delivery of drugs have been considered to reduce these reactions. Our strategy is to coat the surface of biomaterials with a CQ moiety known as an antioxidant. In our study, the scaffolds implanted in the peritoneal cavity show an acute inflammation inhibition effect. Immunostaining of monocyte and macrophage presents significantly reduced surface fluorescence of coated scaffold compared to the uncoated one, which is expected to prevent fibrous tissue formation and lower the probability of implant failure.

The most common cause of ONFH is known to be long-term glucocorticoid steroid use[113]. Furthermore, overuse of glucocorticoids elevates ROS production that exceeds physiological conditions, which exerts oxidative stress on bone tissue[114]. And it is hypothesized that elevated ROS causes bone loss or osteonecrosis by excessive activation of osteoclasts with increasing pro-inflammatory cytokines[115]. Thus, we suggest that scavenging the ROS ability of our antioxidant-coated scaffold can contribute to alleviating one factor of disease beyond simple bone regenerative

implant. It is investigated in vitro and in vivo tests, ROS reduction assay, and decreased pro-inflammatory cytokine expression such as IL-1β, and TNF-α were confirmed using WH_CQ scaffold. Additionally, in a rabbit post-CD model, CD alone group shows a large increase in TNF-α. This can be inferred that further progression of ONFH may occur at the CD lesion. We hold that our WH_CQ scaffold can achieve an ameliorative effect in the post-CD site.

Despite our promising results, more thorough in-depth research needs to be done. Treatment of ONFH requires long-term evaluation on a yearly basis, and our study does not contain such results and there was a lack of more separate comparisons between antioxidant coated and uncoated groups. The progression of the disease obstructs blood flow, resulting in insufficient nutrient supply, and goes through the process of necrosis. This requires understanding and assessment of vessel formation and modification to increase angiogenesis in further study. Functionalization of biomaterials, the addition of stem cells, or blood vessel growth factor (ex. VEGF) supplements might be able to improve therapeutic outcomes. Our follow-up study is expected to focus on the long-term construction of ONFH models and experiments on the enhancement of angiogenesis. It is also necessary to conduct comparative studies with previous bioactive graft materials such as Hap and TCP, etc., to improve relevant data.

Chapter 5. Conclusion

TTCP/WH incorporated functional bone cement is expected to be a better choice for the treatment of osteoporotic vertebral compression fractures in the future due to its excellent biocompatibility, osteoconductivity, and ability to promote bone formation. Antioxidant-coated multifunctional WH scaffold possesses unique biological properties of WH, has excellent bone regeneration ability, promotes the microvascular generation, and reduces ROS and pro-inflammation cytokine expression. It is expected to be a new idea and method for early treatment of the femoral head in the future.

In summary, WH with physiologically active functions and customized biomaterials based on it not only plays a positive role in treating skeletal diseases but also has its own characteristics. The results of this study provide a deeper understanding and experimental basis for whitlockite ceramic-based biomaterials and are expected to be widely used in the medical field in the future.

Acknowledgment:

This study was supported by the Korea Medical Device Development Fund grant funded by the Korea government (the Ministry of Science and ICT)(Project Number:202012E13) and the multidisciplinary research grant-in-aid from the Seoul Metropolitan Government Seoul National University(SMG-SNU) Boramae Medical Center(Project number:04-2022-0041).

Chapter 6. Reference

1. Dorozhkin SV. Bioceramics of calcium orthophosphates. *Biomaterials*. 2010;31:1465-1485.
2. Wojciech Suchanek MY. Processing and properties of hydroxyapatite-based biomaterials for use as hard tissue replacement implants. *J Mater Res*. 1998;13:94-117.
3. R Z LeGeros SL, R Rohanizadeh, D Mijares, J P LeGeros. Biphasic calcium phosphate bioceramics: preparation, properties and applications. *J Mater Sci Mater Med*. 2003;14(3):201-209.
4. Gethin Rh Owen MD, Hannu Larjava. Hydoxyapatite/beta-tricalcium phosphate biphasic ceramics as regenerative material for the repair of complex bone defects. *J Biomed Mater Res B Appl Biomater*. 2018;106(6):2493-2512.
5. J M Bouler PP, O Gauthier, E Verron. Biphasic calcium phosphate ce- ramics for bone reconstruction: a review of biological response. *Acta Biomater*. 2017;53:1-12.
6. T. V. Thamaraiselvi SR. Biological Evaluation of Bioceramic Materials - A Review. *Trends Biomater Artif Organs*. 2004;18 (3):9-17.
7. Vallet-Regía M. Ceramics for medical applications. *J Chem Soc Dalton Trans* 2001;2 (2):97-108.
8. Akira Ogose TH, Hiroyuki Kawashima, Naoki Kondo, Wenguang Gu, Takeshi Kamura, Naoto Endo. Comparison of hydroxyapatite and beta tricalcium phosphate as bone substitutes after excision of bone tumors. *J Biomed Mater Res B Appl Biomater* 2005;72(1):94-101.
9. S. Padilla R, J, Sanchez-Salcedo, S. Hydroxyapatite/SiO2-CaO-P2O5 glass

materials: in vitro bioactivity and biocompatibility. *Acta Biomater*. 2006;2:331-342.

10. Gautam Gupta SK, Ahmed El-Ghannam. Dissolution kinetics of a Si-rich nanocomposite and its effect on osteoblast gene expression *J Biomed Mater Res A*. 2007;80(2):486-496.
11. Hench LL. Bioceramics: from concept to clinic. *J Am Ceram Soc* 2005;74:1487-1510.
12. YuanZhe Jin GZ, HaeLin Jang, KyungMee Lee, JaeHyup Lee Whitlockite Promotes Bone Healing in Rabbit Ilium Defect Model. *J Med Biol Eng*. 2019;39:944-951.
13. Hwan D Kim HLJ, HyoYong Ahn, Hye Kyoung Lee, Jungha Park, EunSeo Lee, Eunjee A Lee, YongHoon Jeong, DoGyoon Kim, Ki Tae Nam, Nathaniel S Hwang. Biomimetic whitlockite inorganic nanoparticles-mediated in situ remodeling and rapid bone regeneration. *Biomaterials*. 2017;112:31-43.
14. Sara Castiglioni AC, Walter Albisetti, Jeanette A M Maier. Magnesium and osteoporosis: current state of knowledge and future research directions. *Nutrients*. 2013;5(8):3022-3033.
15. JeongKui Ku IH, BuKyu Lee, PilYoung Yun, JeongKeun Lee. Dental alloplastic bone substitutes currently available in Korea. *J Korean Assoc Oral Maxillofac Surg* 2019;45(2) 51-67.
16. Xiashiyao Zhang TK, Peiqing Liang, Yong Tang, Changyun Quan. Biological Activity of an Injectable Biphasic Calcium Phosphate/PMMA Bone Cement for Induced Osteogensis in Rabbit Model. *Macromol Biosci* 2018;18(3)
17. Céline Robo GH-B, Malin Nilsson, Cecilia Persson. In vivo response to a low-modulus PMMA bone cement in an ovine model. *Acta Biomater*. 2018;72:362-370.
18. Alberto J Ambard LM. Calcium phosphate cement: review of mechanical and biological properties. *J Prosthodont*. 2006;15(5):321-328.

19. Eric Larson LCJ, Stuart B Goodman, KyungHoi Koo, Quanjun Cui. Early-stage osteonecrosis of the femoral head: where are we and where are we going in year 2018? *Int Orthop*. 2018;42:1723-1728.
20. Lu Cao CG, Jifei Chen, Zenggan Chen, Zuoqin Yan. Free vascularized fibular grafting improves vascularity compared with Core decompression in femoral head osteonecrosis: a randomized clinical trial. *Clin Orthop Relat Res*. 2017;475(9):2230-2240.
21. Todd P Pierce JJJ, Randa K Elmallah, Carlos J Lavernia, Michael A Mont, James Nace. A current review of core decompression in the treatment of osteonecrosis of the femoral head. *Curr Rev Musculoskelet Med*. 2015;8(3):228-232.
22. QuanZhe Liu JK, MinJoon Cho, SuHyeon Kim, Bin Xu, Sivashanmugam Amirthalingam, Nathaniel S. Hwang, JaeHyup Lee. Bioactive Magnesium-Based Whitlockite Ceramic as Bone Cement Additives for Enhancing Osseointegration and Bone Regeneration. *Mater Des*. 2023;229:111914.
23. Suk-Joong Lee JL, HyunJoo Lee, Ji Won Oh, Il-Hyung Park. Pullout strength of pedicle screws using cadaveric vertebrae with or without artificial demineralization. *Spine J*. 2021;21(9):1580-1586.
24. Jae Hyup Lee U-OJ, Do-Hwan Jeon, Bong-Soon Chang, and Choon-Ki Lee. Quantitative Comparison of Novel CaO-SiO2-P2O5-B2O3 Glass-Ceramics(BGS-7) with Hydroxyapatite as Bone Graft Extender in Rabbit Ilium. *TISSUE ENG REGEN MED*. 2010;7:540-547.
25. Brian Hutton GS, Deborah M Caldwell, Anna Chaimani, Christopher H Schmid, Chris Cameron, John P A Ioannidis, Sharon Straus, Kristian Thorlund, Jeroen P Jansen, Cynthia Mulrow, Ferrán Catalá-López, Peter C Gøtzsche, Kay Dickersin, Isabelle

Boutron, Douglas G Altman, David Moher. The PRISMA extension statement for reporting of systematic reviews incorporating network meta-analyses of health care interventions: checklist and explanations. *Ann Intern Med*. 2015;162(11):777-784.

26. Julian P T Higgins DGA, Peter C Gøtzsche, Peter Jüni, David Moher, Andrew D Oxman, Jelena Savovic, Kenneth F Schulz, Laura Weeks, Jonathan A C Sterne; Cochrane Bias Methods Group; Cochrane Statistical Methods Group. The Cochrane Collaboration ' s tool for assessing risk of bias in randomised trials. *BMJ*. 2011;343:d5928.
27. Chaimani A HJ, Mavridis D, Spyridonos P, Salanti G. Graphical tools for network meta-analysis in STATA. *PLoS One*. 2013;8(10):e76654.
28. W I. Multivariate random-effects meta-regression: updates tomvmeta. *Stata J*. 2011;11:255-270.
29. Georgia Salanti AEA, John P A Ioannidis. Graphical methods and numerical summaries for presenting results from multiple-treatment meta-analysis: an overview and tutorial. *J Clin Epidemiol*. 2011;64(2):163-171.
30. Richard D Riley JPTH, Jonathan J Deeks. Interpretation of random effects meta-analyses. *BMJ*. 2011;10:342:d549.
31. Quanzhe Liu BX, MinJoon Cho, JaeHyup Lee. Characteristics of Osteocyte and bone microstructure changes in Steroid-Induced Osteonecrosis of the Femoral Head: In Novel Exper imental Rabbit Models. *Preprint at https://doiorg/1021203/rs3rs-1809628/v1* 2022;
32. Jennifer McKenzie CS, Kannan Karuppaiah, Joshua Langberg, Matthew J Silva, David M Ornitz. Osteocyte Death and Bone Overgrowth in Mice Lacking Fibroblast Growth Factor Receptors 1 and 2 in Mature Osteoblasts and Osteocytes. *J Bone Miner Res*

2019;34(9):1660-1675.

33. Keyun Peng YW, Jifeng Zhu, Chengling Li, Ziming Wang. Repair of non-traumatic femoral head necrosis by marrow core decompression with bone grafting and porous tantalum rod implantation. *Pak J Med Sci*. 2020;36(6):1392-1396.
34. Mengyuan Li YM, Guangtao Fu, Ruiying Zhang, Qingtian Li, Zhantao Deng, Minghao Zheng, Qiujian Zheng. 10-year follow-up results of the prospective, double-blinded, randomized, controlled study on autologous bone marrow buffy coat grafting combined with core decompression in patients with avascular necrosis of the femoral head. *Stem Cell Res Ther*. 2020;11(1):287.
35. Baijun Hu DG, Yihe He. Efficacy of fibula fixation in the early treatment of osteonecrosis of the femoral head and its effects on local microcirculation, articular surface collapse, joint pain and function. *J Musculoskelet Neuronal Interact*. 2018;18(1):55-61.
36. Jean Philippe Hauzeur VDM, Etienne Baudoux, Michel Malaise , Yves Beguin, Valérie Gangji. Inefficacy of autologous bone marrow concentrate in stage three osteonecrosis: a randomized controlled double-blind trial. *Int Orthop*. 2018;42(7):1429-1435.
37. Wojciech Pepke PK, Nicholas A Beckmann, Patricia Janicki, Marcus Egermann. Core decompression and autologous bone marrow concentrate for treatment of femoral head osteonecrosis: a randomized prospective study. *Orthop Rev (Pavia)*. 2016;8(1):6162.
38. Deqiang Li ML, Peilai Liu, Yuankai Zhang, Liang Ma, Fei Xu. Core decompression or quadratus femoris muscle pedicle bone grafting for nontraumatic osteonecrosis of the femoral head: a randomized control study. *Indian J Orthop*. 2016;50:629-635.

39. Reza Mostafavi Tabatabaee SS, Javad Parvizi, Seyed Mohammad Javad Mortazavi, Mahmoud Farzan. Combining concentrated autologous bone marrow stem cells injection with Core decompression improves outcome for patients with early-stage osteonecrosis of the femoral head: a comparative study. *J Arthroplasty*. 2015;30(9 Suppl):11-15.
40. Haixiong Miao DY, Weiguo Liang, Yicun Yao. Effect of osteonecrosis intervention rod versus Core decompression using multiple small Drill holes on early stages of necrosis of the femoral head: a prospective study on a series of 60 patients with a minimum 1-year-follow-up. *Open Orthop J*. 2015;9:179-184.
41. Yuanchen Ma TW, Junxing Liao, Honglin Gu, Xinpeng Lin, Qing Jiang, Max K Bulsara, Minghao Zheng, Qiujian Zheng. Efficacy of autologous bone marrow buffy coat grafting combined with core decompression in patients with avascular necrosis of femoral head: a prospective, doubleblinded, randomized, controlled study. *Stem Cell Res Ther*. 2014;5(5):115.
42. Dewei Zhao DC, Benjie Wang, Fengde Tian, Lin Guo, Lei Yang, Baoyi Liu, Xiaobing Yu. Treatment of early stage osteonecrosis of the femoral head with autologous implantation of bone marrow-derived and cultured mesenchymal stem cells. *Bone*. 2012;50(1):325-330.
43. Ramesh Kumar Sen SKT, Sameer Aggarwal, Neelam Marwaha, Ratti Ram Sharma, Niranjan Khandelwal. Early results of core decompression and autologous bone marrow mononuclear cells instillation in femoral head osteonecrosis: a randomized control study. *J Arthroplasty*. 2012;27(5):679-686.
44. Valérie Gangji VDM, Jean-Philippe Hauzeur. Autologous bone marrow cell implantation in the treatment of non-traumatic osteonecrosis of the femoral head:

five year follow-up of a prospective controlled study. *Bone*. 2011;49(5):1005-1009.

45. Lynne D Neumayr CA, Ann N Earles, Harry E Jergesen, Charles M Haberkern, Bamidele F Kammen, Paul A Nancarrow, Eric Padua, Meredith Milet, Bernard N Stulberg, Roger A Williams, Eugene P Orringer, Nora Graber, Shanda M Robertson, Elliott P Vichinsky; National Osteonecrosis Trial in Sickle Cell Anemia Study Group. Physical therapy alone compared with core decompression and physical therapy for femoral head osteonecrosis in sickle cell disease. Results of a multicenter study at a mean of three years after treatment. *J Bone Joint Surg Am*. 2006;88(12):2573-2582.
46. Ching-Jen Wang F-SW, Chung-Cheng Huang, Kuender D Yang, Lin-Hsiu Weng, Hsuan-Ying Huang. Treatment for osteonecrosis of the femoral head: comparison of extracorporeal shock waves with core decompression and bone-grafting. *J Bone Joint Surg Am*. 2005;87(11):2380-2387.
47. K H Koo RK, G H Ko, H R Song, S T Jeong, S H Cho. Preventing collapse in early osteonecrosis of the femoral head. A randomised clinical trial of core decompression. *J Bone Joint Surg Br*. 1995;77:870-874.
48. B N Stulberg AWD, T W Bauer, M Levine, K Easley. Osteonecrosis of the femoral head. A prospective randomized treatment protocol. *Clin Orthop Relat Res*. 1991;268:140-151.
49. Marbod Weber HS, Sonia Golombek, Ludmilla Hann, Christian Schlensak, Hans P Wendel, Meltem Avci-Adali. Blood-Contacting Biomaterials: In Vitro Evaluation of the Hemocompatibility. *Front Bioeng Biotechnol*. 2018;6:99.
50. Kan Zhan HE, Naoko Yoshie. Antioxidant and Adsorption Properties of Bioinspired Phenolic Polymers: A Comparative Study of Catechol and Gallol. *Acs Sustain Chem*

Eng 2016;4(7):3857-3863.

51. L.R.C. Barclay CEE, M.R. Vinqvist. Media effects on antioxidant activities of phenols and catechols. *J Am Chem Soc* 1999;121(26):6226-6231.
52. Yang Yimin RZ, Ma Wei, Rajiv Jha. Current status of percutaneous vertebroplasty and percutaneous kyphoplasty--a review. *Med Sci Monit*. 2013;19:826-836.
53. Enrica Verné MB, Marta Miola, Giovanni Maina, Carlotta Bianco, Andrea Cochis, Lia Rimondini. Composite bone cements loaded with a bioactive and ferrimagnetic glass-ceramic: Leaching, bioactivity and cytocompatibility. *Mater Sci Eng C Mater Biol Appl*. 2015;53:95-103.
54. Ling Yu KX, Changtian Gong, Jingteng Chen, Wei Li, Yanan Zhao, Weichun Guo, Honglian Dai. An injectable bioactive magnesium phosphate cement incorporating carboxymethyl chitosan for bone regeneration. *Int J Biol Macromol*. 2020;160:101-111.
55. Cairong Li JS, Keda Shi, Jing Long, Long Li, Yuxiao Lai, Ling Qin. Preparation and evaluation of osteogenic nano-MgO/PMMA bone cement for bone healing in a rat critical size calvarial defect. *J Mater Chem B*. 2020;8(21):4575-4586.
56. G Baroud MS, T Steffen. Influence of mixing method on the cement temperature-mixing time history and doughing time of three acrylic cements for vertebroplasty. *J Biomed Mater Res B Appl Biomater*. 2004;68(1):112-116.
57. M A Rauschmann DvS, K-D Thomann, D Scale. Complications of vertebroplasty. *Orthopade*. 2004;33(1):40-47.
58. A Castaldini AC. Setting properties of bone cement with added synthetic hydroxyapatite. *Biomaterials*. 1985;6(1):55-60.
59. Kefeng Luo GJ, Jinjin Zhu, Bin Lu, Jiye Lu, Kai Zhang, Xiumei Wang, Fu-Zhai Cui.

Poly(methyl methacrylate) bone cement composited with mineralized collagen for osteoporotic vertebral compression fractures in extremely old patients. *Regen Biomater*. 2020;7(1):29-34.

60. Paul A Hulme JK, Stephen J Ferguson, Ulrich Berlemann. Vertebroplasty and kyphoplasty: a systematic review of 69 clinical studies. *Spine (Phila Pa 1976)*. 2006;31(17):1983-2001.
61. Xi Wang JK, Yang Yue, XiSheng Weng, ZhiYe Qiu, XiFeng Zhang. Clinical outcome comparison of polymethylmethacrylate bone cement with and without mineralized collagen modification for osteoporotic vertebral compression fractures. *Medicine (Baltimore)*. 2018;97(37):e12204.
62. Qinghua Xiao YZ, Zhen Qu, Zhen Zhang, Keliang Wu, Xiaosheng Lin. Association Between Bone Cement Augmentation and New Vertebral Fractures in Patients with Osteoporotic Vertebral Compression Fractures: A Systematic Review and Meta-Analysis. *World Neurosurg*. 2021;153:98-108.e3.
63. Xin Sun ZW, Dan He, Kangping Shen, Xingzhen Liu, Haiyan Li, Wenjie Jin. Bioactive injectable polymethylmethacrylate/silicate bioceramic hybrid cements for percutaneous vertebroplasty and kyphoplasty. *J Mech Behav Biomed Mater* 2019;96:125-135.
64. Atsushi Sugino TM, Giichiro Kawachi, Koichi Kikuta, Chikara Ohtsuki. Relationship between apatite-forming ability and mechanical properties of bioactive PMMA-based bone cement modified with calcium salts and alkoxysilane. *J Mater Sci Mater Med*. 2008;19(3):1399-1405.
65. M Portigliatti-Barbos PR, L Salvadori, S Carando, M Gallinaro. Bone-cement interface: A histological study of aseptic loosening in twelve prosthetic implants. *Ital*

J Orthop Traumatol. 1986;12:499-505.

66. Kenneth A Mann MAM, Richard J Cleary, Dennis Janssen, Nico Verdonschot. Experimental micromechanics of the cement-bone interface. *J Orthop Res*. 2008;26:872-879.
67. Nipun Sodhi AA, Jennifer Etcheson, Nequesha Mohamed, Iciar Davila, Joseph O Ehiorobo, Lynne C Jones, Ronald E Delanois, Michael A Mont. Management of osteonecrosis of the femoral head. *Bone Joint J*. 2020;102-b (7_Supple_B):122-128.
68. David R Marker TMS, Slif D Ulrich, Siddharth Srivastava, Michael A Mont. Do modern techniques improve core decompression outcomes for hip osteonecrosis? *Clin Orthop Relat Res*. 2008;466(5):1093-1103.
69. Zalavras CG LJ. Osteonecrosis of the femoral head: evaluation and treatment. *J Am Acad Orthop Surg*. 2014;22(7):455-464.
70. Brian J McGrory SCY, Richard Iorio, William Macaulay, Richard R Pelker, Brian S Parsley, Steven M Teeny. Current practices of AAHKS members in the treatment of adult osteonecrosis of the femoral head. *J Bone Joint Surg Am*. 2007;89(6):1194-1204.
71. Pengde Kang FP, Bin Shen, Zongke Zhou, Jing Yang. Are the results of multiple drilling and alendronate for osteonecrosis of the femoral head better than those of multiple drilling? A pilot study. *Joint Bone Spine*. 2012;79(1):67-72.
72. YuCai Hong HZ, Tiao Lin, JianBin Shi. Comparison of core decompression and conservative treatment for avascular necrosis of femoral head at early stage: a meta-analysis. *Int J Clin Exp Med*. 2015;8(4):5207-5216.
73. Xu Li XX, Wei Wu. Comparison of bone marrow mesenchymal stem cells and core decompression in treatment of osteonecrosis of the femoral head: a meta-analysis.

Int J Clin Exp Pathol. 2014;7(8):5024-5030.

74. F P Castro Jr RLB. Core decompression and conservative treatment for avascular necrosis of the femoral head: a meta-analysis. *Am J Orthop (Belle Mead NJ)*. 2000;29(3):187-194.
75. M A Mont JJC, A C Fairbank. Core decompression versus nonoperative management for osteonecrosis of the hip. *Clin Orthop Relat Res*. 1996;324:169-178.
76. Michael A Mont JJC, Rafael J Sierra, Lynne C Jones, Jay R Lieberman. Nontraumatic osteonecrosis of the femoral head: where do we stand today? A ten-year update. *J Bone Joint Surg Am*. 2015;97(19):1604-1627.
77. Ahmad Oryan AK, Ali Moshiri, Mohamadreza Baghaban Eslaminejad. Role of Mesenchymal stem cells in bone regenerative medicine: what is the evidence? *Cells Tissues Organs*. 2017;204(2):59-83.
78. Shanhong Fang YL, Peng Chen. Osteogenic effect of bone marrow mesenchymal stem cell-derived exosomes on steroid-induced osteonecrosis of the femoral head. *Drug Des Devel Ther*. 2019;13:45-55.
79. Eric Larson LCJ, Stuart B. Goodman, KyungHoi Koo,Quanjun Cui. Early-stage osteonecrosis of the femoral head: where are we and where are we going in year 2018? *Int Orthop*. 2018;42(7):1723-1728.
80. Goodman SB. The biological basis for concentrated iliac crest aspirate to enhance core decompression in the treatment of osteonecrosis. *Int Orthop*. 2018;42(7):1705-9.
81. Ph Hernigou AH, D Bachir, F Galacteros. The natural history of asymptomatic osteonecrosis of the femoral head in adults with sickle cell disease. *J Bone Joint Surg Am*. 2006;88(12):2565-2572.

82. Zhan Wang QS, FuQiang Zhang, QunLi Zhang, LiGuo Wang, WenJi Wang. Core decompression combined with autologous bone marrow stem cells versus core decompression alone for patients with osteonecrosis of the femoral head: a meta-analysis. *Int J Surg*. 2019;69:23-31.
83. Luca Andriolo GM, Carlos Tobar, Sante Alessandro Altamura, Elizaveta Kon, Giuseppe Filardo. Regenerative therapies increase survivorship of avascular necrosis of the femoral head: a systematic review and meta-analysis. *Int Orthop*. 2018;42(7):1689-1704.
84. Young Wook Lim YSK, Jong Wook Lee, Soon Yong Kwon. Stem cell implantation for osteonecrosis of the femoral head. *Exp Mol Med*. 2013;45(11):e61.
85. PHEMISTER DB. Treatment of the necrotic head of the femur in adults. *J Bone Joint Surg Am*. 1949;31a(1):55-66.
86. Todd P Pierce RKE, Julio J Jauregui, Shiva Poola, Michael A Mont, Ronald E Delanois. A current review of non-vascularized bone grafting in osteonecrosis of the femoral head. *Curr Rev Musculoskelet Med*. 2015;8(3):240-245.
87. Todd P Pierce JJJ, Randa K Elmallah, Carlos J Lavernia, Michael A Mont, James Nace. A current review of core decompression in the treatment of osteonecrosis of the femoral head. *Curr Rev Musculoskelet Med*. 2015;8(3):228-232.
88. Yang Zhang LL, Zhan-jun Shi, Jian Wang, Zhi-han Li. Porous tantalum rod implant is an effective and safe choice for early-stage femoral head necrosis: a meta analysis of clinical trials. *Eur J Orthop Surg Traumatol*. 2013;23(2):211-217.
89. KunChi Hua XY, JiangTao Feng, Feng Wang, Li Yang, Hao Zhang, YongCheng Hu. The efficacy and safety of core decompression for the treatment of femoral head necrosis: a systematic review and meta-analysis. *J Orthop Surg Res*.

2019;14(1):306.

90. Bingli Liu WS, Debo Yue, Zirong Li, Wanshou Guo. Combined tantalum implant with bone grafting for the treatment of osteonecrosis of the femoral head *J Investig Surg*. 2013;26(3):158-162.
91. M Tanzer JDB, J J Krygier, D Karabasz. Histopathologic retrieval analysis of clinically failed porous tantalum osteonecrosis implants. *J Bone Joint Surg Am*. 2008;90(6):1282-1289.
92. William C Eward CAR, James R Urbaniak, Marc J Richard, David S Ruch. The vascularized fibular graft in precollapse osteonecrosis: is long-term hip preservation possible? . *Clin Orthop Relat Res*. 2012;470(10):2819-2826.
93. Shin-Yoon Kim Y-GK, Poong-Taek Kim, Joo-Chul Ihn, Byung-Chae Cho, Kyung-Hoi Koo. Vascularized compared with nonvascularized fibular grafts for large osteonecrotic lesions of the femoral head. *J Bone Joint Surg Am*. 2005;87(9):2012-2018.
94. Anastasios V Korompilias AEB, Marios G Lykissas, Ioannis P Kostas-Agnantis, Panayiotis N Soucacos. Femoral head osteonecrosis: why choose free vascularized fibula grafting. *Microsurgery*. 2011;31(3):223-228.
95. J R Urbaniak PGC, E B Gunneson, J A Nunley. Treatment of osteonecrosis of the femoral head with free vascularized fibular grafting. A long-term follow-up study of one hundred and three hips. *J Bone Joint Surg Am*. 1995;77(5):681-694.
96. Changqing Zhang BZ, Zhengyu Xu, Shuping Sui, Wenqi Song, Dongxu Jin, Huipeng Shi, Kunzheng Wang. Treatment of osteonecrosis of femoral head with free vascularized fibula grafting. *Zhongguo Xiu Fu Chong Jian Wai Ke Za Zhi*. 2004;18(5):367-369.

97. M C Yoo DWC, C S Hahn. Free vascularized fibula grafting for the treatment of osteonecrosis of the femoral head. *Clin Orthop Relat Res*. 1992;277:128-138.

98. Maria Chiara Meloni WRH, Victor Fornasier. Failed vascularized fibular graft in treatment of osteonecrosis of the femoral head. A histopathological analysis. *Joints*. 2016;4(1):24-30.

99. Ji Wang JW, Kai Zhang, Yanfang Wang, Xuanwen Bao. Bayesian network Meta-analysis of the effectiveness of various interventions for nontraumatic osteonecrosis of the femoral head. *Biomed Res Int*. 2018;2018:2790163.

100. R S Weinstein RWN, S C Manolagas. Apoptosis of osteocytes in glucocorticoid-induced osteonecrosis of the hip. *J Clin Endocrinol Metab*. 2000;85(8):2907-2912.

101. Marco Grassi PS, Daniele Massetti, Giuseppe F Papalia, Antonio Gigante. Treatment of avascular osteonecrosis of femoral head by core decompression and platelet-rich plasma: a prospective not controlled study *Int Orthop*. 2020;44(7):1287-1294.

102. Chen Changjun LD, Zhao Xin, Chen Liyile, Wang Qiuru, Kang Pengde Mid- to long-term results of modified non-vascularized allogeneic fibula grafting combined with core decompression and bone grafting for early femoral head necrosis. *J Orthop Surg Res*. 2020;15(1):116.

103. Assem A Sultan AK, Peter Surace, Linsen T Samuel, Mhamd Faour, Nipun Sodhi, Viktor E Krebs, Kim L Stearns, Robert M Molloy, Michael A Mont. The use of non-vascularized bone grafts to treat osteonecrosis of the femoral head: indications, techniques, and outcomes. *Int Orthop*. 2019;43(6):1315-1320.

104. Michael S Shuler MDR, James R Roberson. Porous tantalum implant in early osteonecrosis of the hip: preliminary report on operative, survival, and outcomes results. *J Arthroplasty*. 2007;22(1):26-31.

105. Hae Lin Jang GBZ, Jungha Park, Hwan D Kim, Hae-Ri Baek, Hye Kyoung Lee, Keunho Lee, Heung Nam Han, Choon-Ki Lee, Nathaniel S Hwang, Jae Hyup Lee, Ki Tae Nam. In Vitro and In Vivo Evaluation of Whitlockite Biocompatibility: Comparative Study with Hydroxyapatite and β-Tricalcium Phosphate. *Adv Healthc Mater*. 2016;5(1):128-136.

106. Yifeng Zhang JX, YeChun Ruan, MeiKuen Yu, Micheal O'Laughlin, Helen Wise, Di Chen, Li Tian, Dufang Shi, Jiali Wang, Sihui Chen, Jian Q Feng, Dick Ho Kiu Chow, Xinhui Xie, Lizhen Zheng, Le Huang, Shuo Huang, Kwoksui Leung, Na Lu, Lan Zhao, Huafang Li, Dewei Zhao, Xia Guo, Kaiming Chan, Frank Witte, Hsiao Chang Chan, Yufeng Zheng, Ling Qin. Implant-derived magnesium induces local neuronal production of CGRP to improve bone-fracture healing in rats. *Nat Med* 2016;22(10):1160-1169.

107. Hans E Schoemaker DM, Marcel G Wubbolts. Dispelling the myths--biocatalysis in industrial synthesis. *Science* 2003;299(5613):1694-1697.

108. Chan Hee Lee ESJ, Jin Hyung Lee, Ee Taek Hwang. Immobilization and Stabilization of Enzyme in Biomineralized Calcium Carbonate Microspheres. *Front Bioeng Biotechnol* 2020;8:553591.

109. Sumitra Datta LRC, Yamuna Rani Sriramulu Rajaram. Enzyme immobilization: an overview on techniques and support materials. *Biotech* 2013;3(1):1-9.

110. James M Anderson AR, David T Chang. Foreign body reaction to biomaterials. *Semin Immunol* 2008;20(2):86-100.

111. Y. Onuki UB, F. Papadimitrakopoulos, D.J. Burgess. A review of the biocompatibility of implantable devices: current challenges to overcome foreign body response. *J Diabetes Sci Technol* 2008;2(6):1003-1015.

112. Zeeshan Sheikh PJB, Oriyah Barzilay, Noah Fine, Michael Glogauer. Macrophages, Foreign Body Giant Cells and Their Response to Implantable Biomaterials. *Materials (Basel)*. 2015;8(9):5671-5701.

113. Daniel Petek DH, Domizio Suva. Osteonecrosis of the femoral head: pathophysiology and current concepts of treatment. *EFORT Open Rev* 2019;4(3):85-97.

114. Kai Chen YL, Jianbo He, Nathan Pavlos, Chao Wang, Jacob Kenny, Jinbo Yuan , Qingwen Zhang, Jiake Xu, Wei He. Steroid-induced osteonecrosis of the femoral head reveals enhanced reactive oxygen species and hyperactive osteoclasts. *Int J Biol Sci* 2020;16(11):1888-1900.

115. Xinghuo Wu WX, Xiaobo Feng, Yu He, Xianzhe Liu, Yong Gao, Shuhua Yang, Zengwu Shao, Cao Yang, Zhewei Ye. TNF-a mediated inflammatory macrophage polarization contributes to the pathogenesis of steroid-induced osteonecrosis in mice. *Int J Immunopathol Pharmacol* 2015;28(3):351-361.

116. Quanzhe Liu WG, Rui Li, JaeHyup Lee. Efficacy of various core decompression techniques versus non-operative treatment for osteonecrosis of the femoral head: a systemic review and network meta-analysis of randomized controlled trials. *BMC Musculoskelet Disord*. 2021;22(1):948.

Table 1. Groups and materials for bone cements.

	Group 1 PMMA	Group 2 HEMA	Group 3 TTCP	Group 4 TTCP/WH
Powder	PMMA	PMMA	PMMA (60%) TTCP (40%)	PMMA (60%) TTCP (20%) + WH (20%)
Liquid	MMA	MMA (80v/v%) + HEMA (20v/v%)		
P : L (g/ml)	2:1			
Other	Barium sulfate, Benzoyl peroxide, N, N-dimethyl-p-toluidine, Hydroquinone			

Table 2. Medline via OVID search strategy.

MEDLINE via OVID search strategy	
No.	**Query**
1	exp Orthopedics/su
2	exp Orthopedic Procedures
3	exp Joints/su
4	("Orthopedic Procedure*" or "Orthopaedic Procedure*").ab,ti.
5	((Orthopedic or Orthopaedic) adj3 Surger*).ab,ti.
6	"orthopedic operat*".ab,ti. (385)
7	("surgical orthopedic" or "surgical orthopaedic").ab,ti.
8	1 or 2 or 3 or 4 or 5 or 6 or 7
9	exp Femur Head Necrosis
10	(osteonecrosis adj3 femoral head).ab,ti.
11	(osteonecrosis adj3 femur head).ab,ti.
12	(necrosis adj3 femoral head).ab,ti.
13	(necrosis adj3 femur head).ab,ti.
14	"ONFH".ab,ti.
15	9 or 10 or 11 or 12 or 13 or 14
16	8 and 15 (3704)
17	limit 16 to humans

Table 3. Basic characteristics of the included studies[116].

No.	Author	Year	Intervention	No.P	No.Hip	Sex(M/F)	Age	Stage(I-IV) ARCO	Risk factors				Follow-up
									Steroid	Alcohol	Idiopathic	others	
1	Peng, K.	2020	CD+BG	30	38	17:13	46.7±13.9	11:19:0:0	16	8	0	6	1years
			CD+TI	30	38	15:15		13:17:0:0	17	6	0	7	
2	Hauzeur, J. P	2018	CD	19	23	13:6	49.7 ± 3.2	0:0:23:0	13	7	3	0	2 years
			CD+CT	19	23	14:5	48.0 ± 2.8	0:0:23:0	12	8	1	2	
3	Cao, L.	2017	CD+BG	21	21	16:5	31 ± 6	3:13:5:0	7	8	6	0	3 years
			VBG		21			2:13:6:0					
4	Pepke, W.	2016	CD	24	14	8:6	44.5±3.3	0:14:0:0	NR				2 years
			CD+CT		11	6:5	44.3±3.4	0:11:0:0					
5	Tabatabaee, R. M.	2015	CD	13	14	10:4	26.8 ± 5.8	2:7:5:0	9	0	5	0	2 years
			CD+CT	14	14	9:5	31 ± 11.4	3:9:2:0	10	0	4	0	
6	Zhao, D.	2012	CD	50	51	26:24	33.8±7.70	2:49:0:0	13	7	13	17	5 years
			CD+CT	50	53	27:23	32.7±10.5	3:48:0:0	10	11	16	13	
7	Wang	2005	Non-surg	23	29	20:3	39.8 ± 12.1	3:10:16:0	2	16	0	5	2 years
			CD+BG	25	28	23:2	39.9 ± 9.3	2:17:9:0	2	16	0	7	
8	Gangji	2011	CD	19	11	10:9	45.7±2.8	2:9:0:0	9	1	1	0	5years
			CD+CT		13		42.2±2.6	2:11:0:0	11	1	1	0	
9	Sen, R. K.	2012	CD	40	25	18:7	65.7 ± 15.2	Stage (I or II)	20	8	2	21	2 years
			CD+CT		26	19:7	66.2 ± 13.0						
								Ficat					
10	Ma, Y.	2014	CD+BG	18	24	13:5	35 ± 9.8	4:15:5:0	13	3	6	0	2 years
			CD+BG+CT	21	25	15:6		3:17:5:0	13	4	6	0	
11	Li, MY	2020	CD+BG	14	20	10:4	38.2 ± 8.1	0:11:9:0	9	5	6	0	10 years
			CD+BG+CT	17	21	12:5	34.1 ± 8.0	0:11:10:0	10	6	5	0	
12	Stulberg BN,	1991	CD	19	28	NR	38.6	18:14:21:0	10	3	4	2	18
			Non-surg	17	25				8	8	1	0	months
13	Deqiang Li,	2016	CD+BG	20	23	27:12	36.5 (23-59)	21:26:0:0	8	23	0	8	2.5 years
			VBG	19	24								
								Steinberg					
14	Neumayr LD,	2006	CD	17	17	8:9	24.67	2:5:10:0	NR				3 years
			Non-surg	21	21	11:10	26.41	8:6:7:0					
15	Miao H	2015	CD+TI	30	36	12:18	32.6±6.3	16:20:0:0	22	4	7	0	18
			CD	30	34	13:17	35.2±5.8	14:20:0:0	24	5	8	0	months
16	Koo KH	1995	CD+BG	17	18	16:1	45	10:7:1:0	2	14	2	0	2years
			Non-surg	17	19	16:1	48	12:4:3:0	2	17	0	0	
17	Hu, B. J.	2018	CD	65	65	44:21	40.38±6.63	NR	NR				4 years
			CD+BG	65	65	46:19	40.83±6.73						

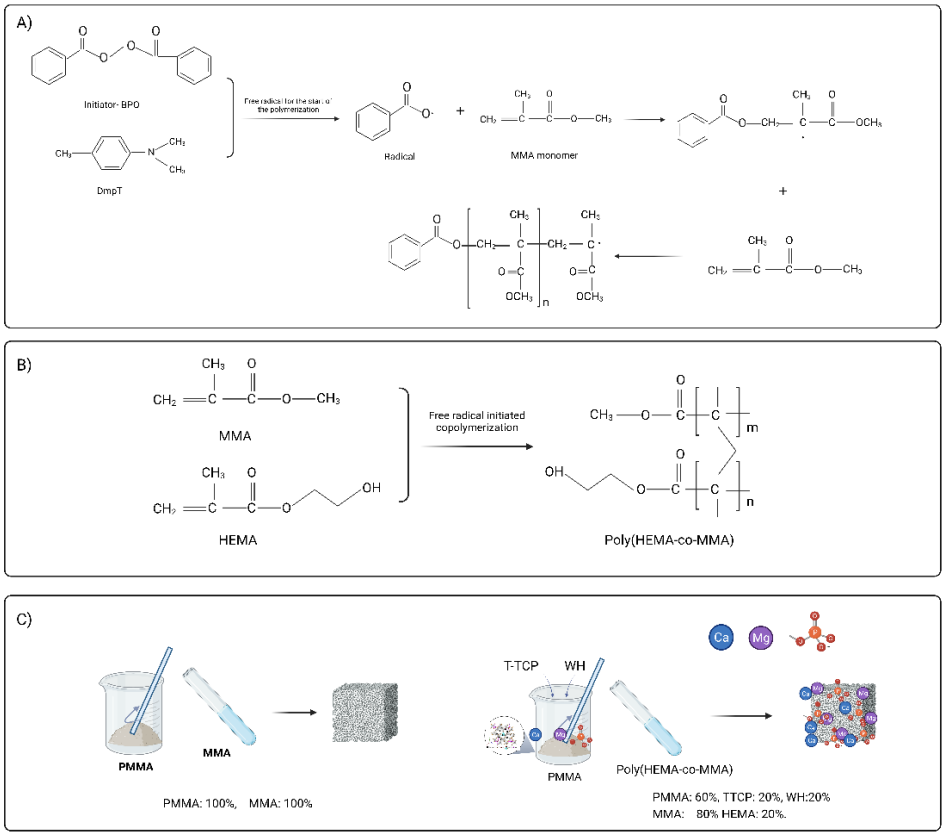

Figure 1. Powder and liquid chemical reaction and material preparation.

A) Radical polymerization of MMA to PMMA; B) Schematic representation of free radical initiated copolymerization of HEMA and MMA. C) Bone cement preparation and synthesis. (Poly methyl methacrylate (PMMA); Tetra calcium phosphate (TTCP); Whitlockite (WH); Hydroxyethyl Methacrylate (HEMA); Methyl methacrylate (MMA); Benzoyl peroxide(BPO)).

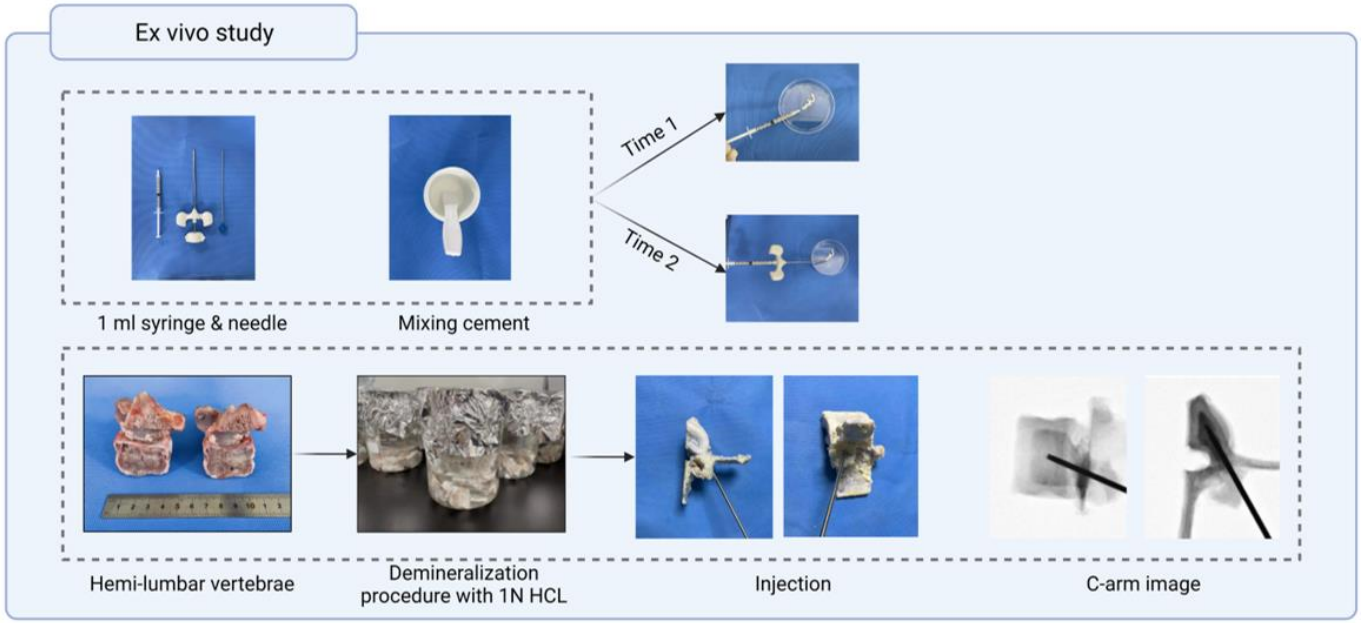

Figure 2. Cement injection and operational working time.

Time 1: suitable for pushing into the vertebral body with a vertebroplasty injection needle. Time 2: suitable for pushing with a 1ml syringe after mixing. (Temperature:24±1℃ ; Humidity: 45.7±2%; VAV(variable Air volume):100%).

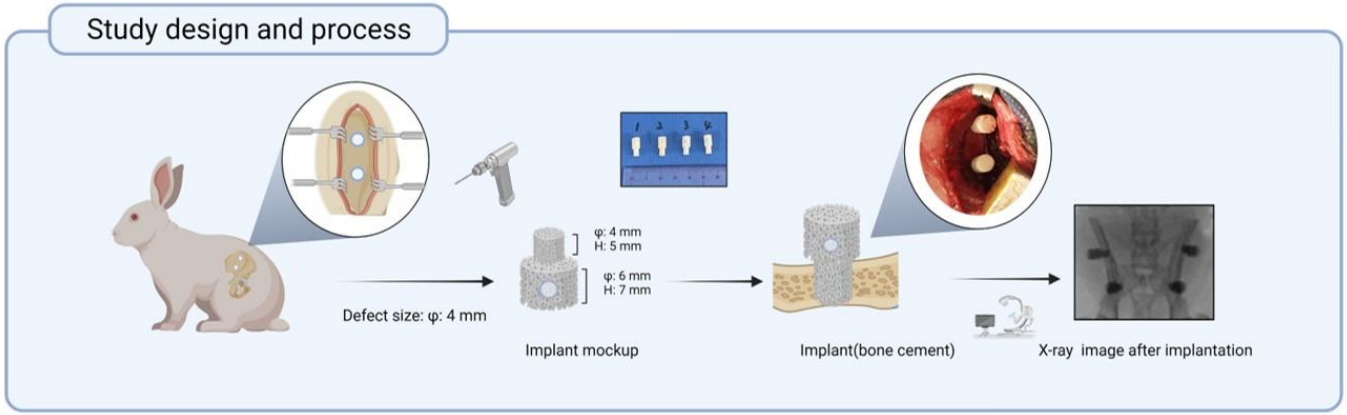

Figure 3. Study design of in vivo model in part 1.

Test implants: The 7 mm long cylindrical bar with a diameter of 6 mm was connected to a 5 mm cylindrical bar of diameter 4mm.

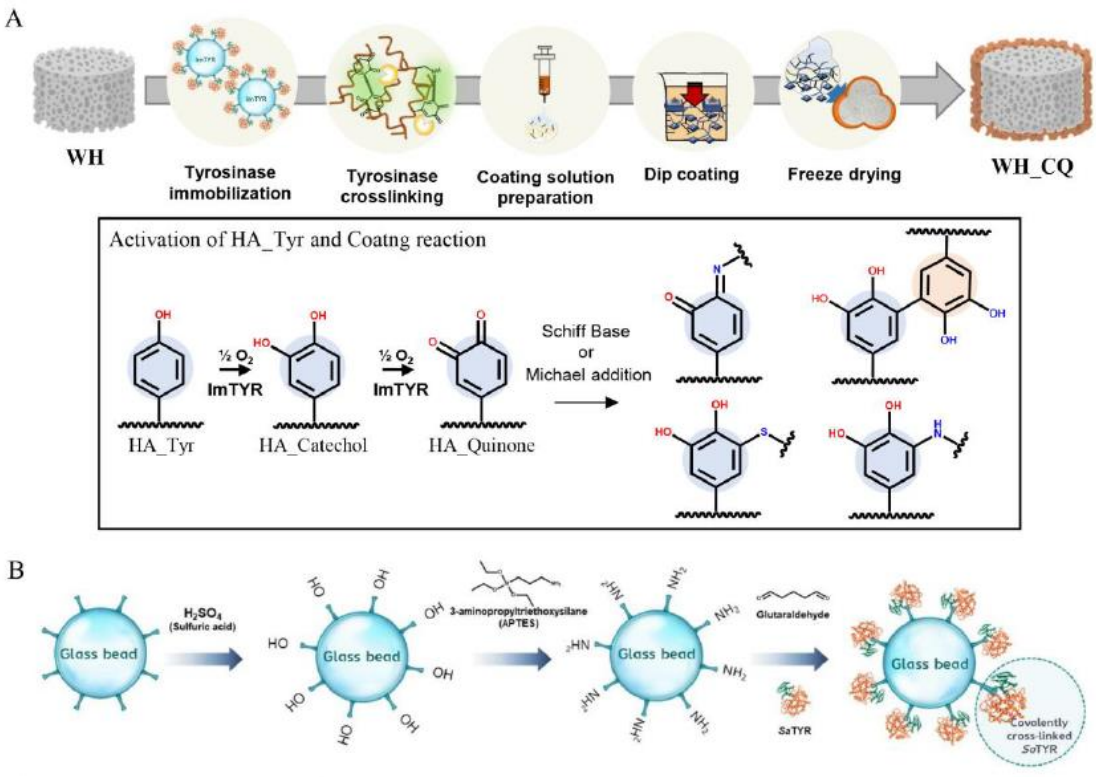

Figure 4. Scaffold fabrication and HA_CQ coating.

A) Schematic illustration of scaffold fabrication steps; B) Schematic figure of the immobilization on the glass bead by covalent bond.

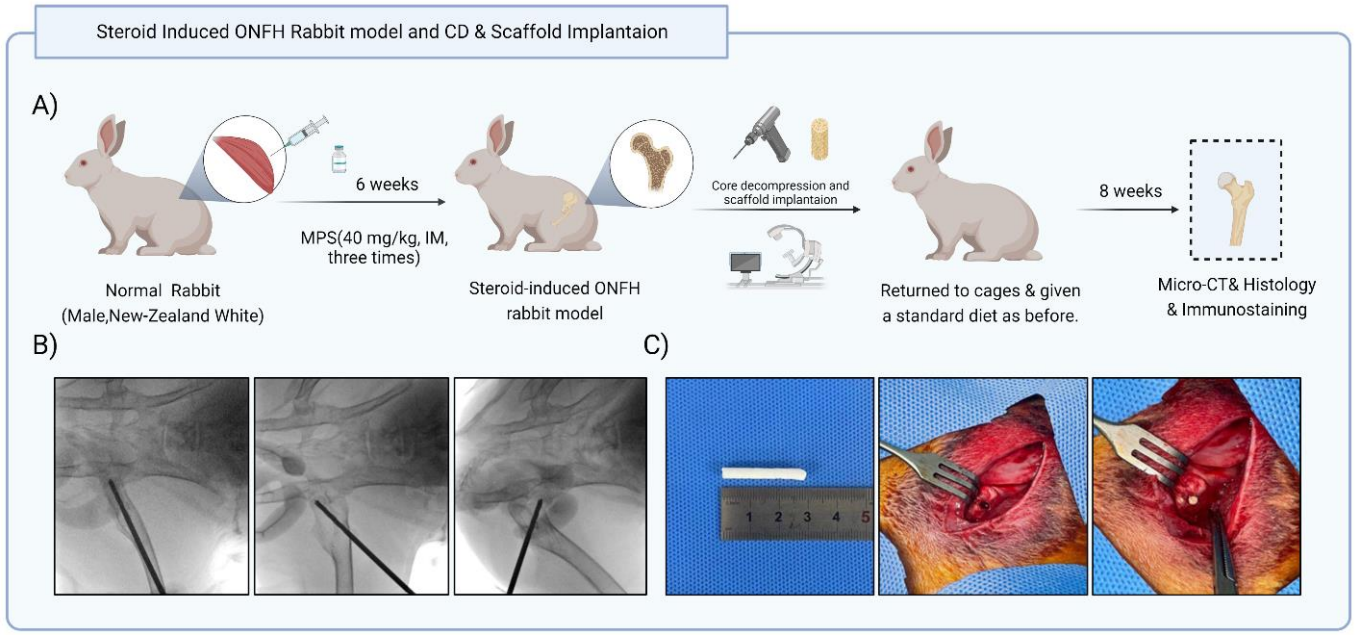

Figure 5. Study design and surgical procedures in part 2.

A) Steroid-induced ONFH rabbit model and surgery intervention scheme. B) X-ray image of core decompression (CD) procedures. C) Scaffold and surgical approach.

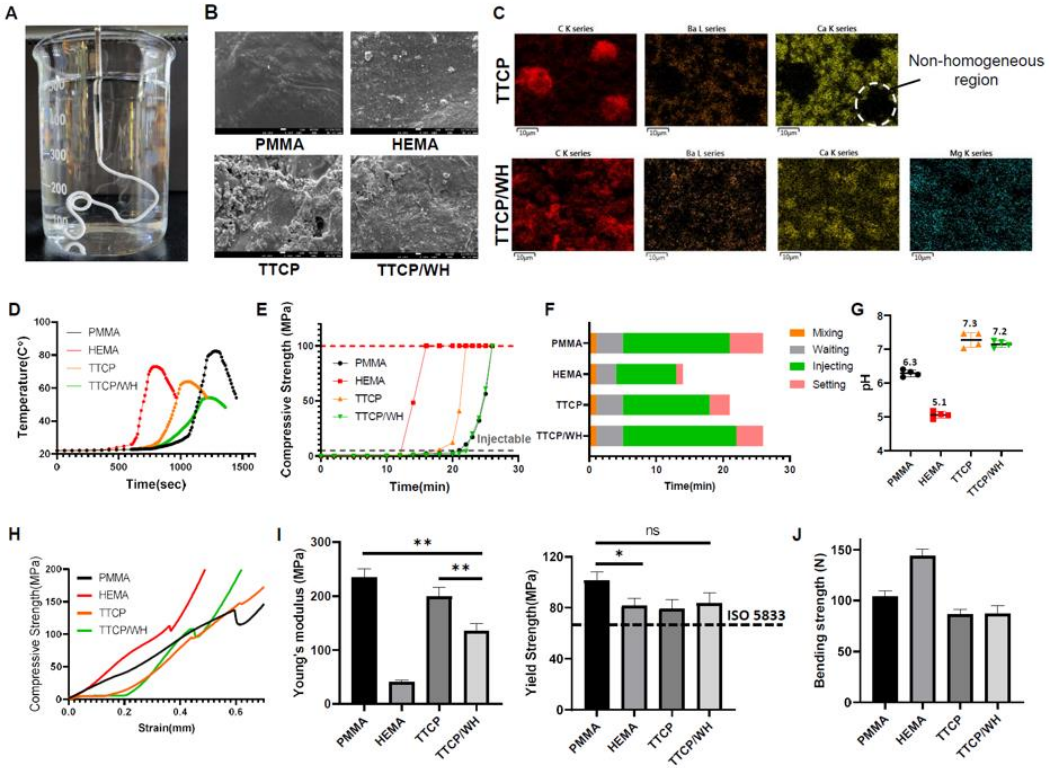

Figure 6. Fabrication and characteristics of TTCP/WH bone cement.

A) Picture of TTCP/WH cement injection into PBS. B) SEM images of each cement group C) EDS images of TTCP/WH cement D) Temperature measurement of cement from mixing to setting E) Compressive strength measurement of cement during reaction F) Adjusted process time interval of cement based on strength G) Surface pH measurement of cements H) Compressive strength of set cements I) (Left) Young's modulus of cements (Right) Yield strength of cements J) 3-points Bending strength of cements.

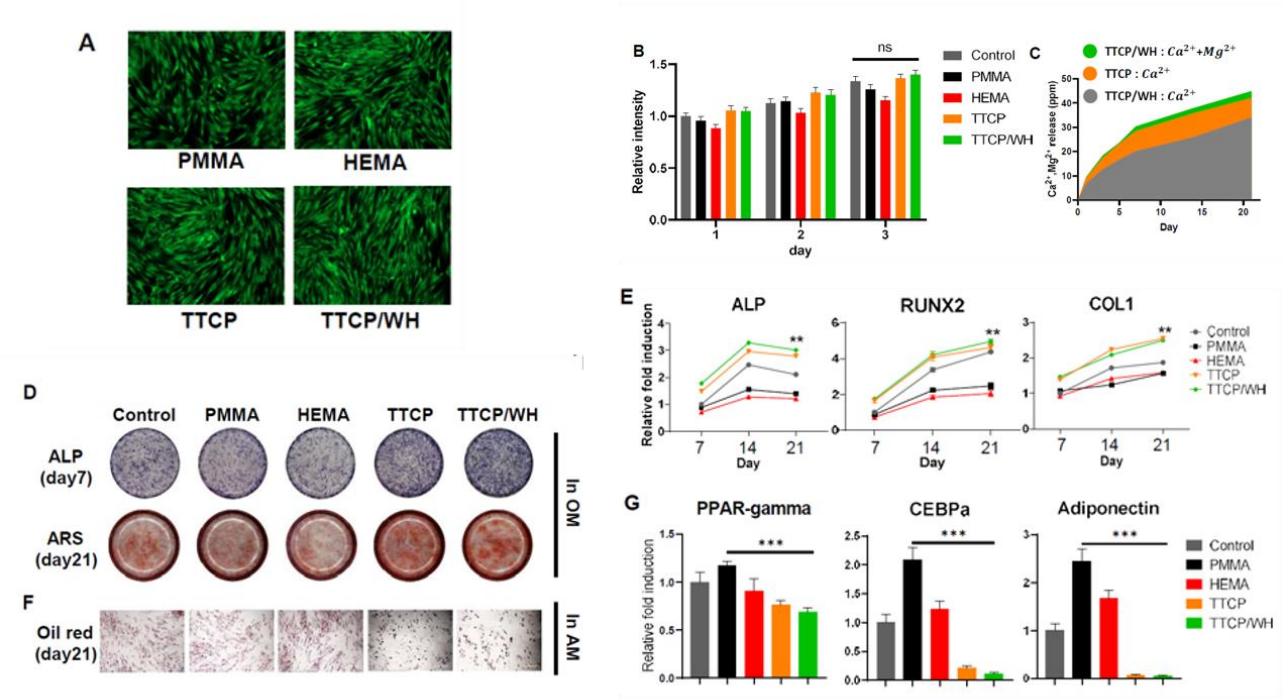

Figure 7. In vitro osteogenic and anti-adipogenic effect of TTCP/WH bone cement.

A) Live/Dead staining assay with cement conditioned medium (0.1g/ml) B) Cell viability test with prestoblue using cement conditioned medium C) Cation (Calcium, magnesium) release from cement scaffold (ppm). D) ALP, ARS staining of hBMSCs with osteogenic cement conditioned medium. E) Osteogenic gene expression of hBMSCs cultured using osteogenic cement conditioned medium at day 7, 14, 21. F) Oil red O staining of hBMSCs with adipogenic cement conditioned medium. G) Adipogenic gene expression of hBMSCs cultured using adipogenic cement conditioned medium at day 21.

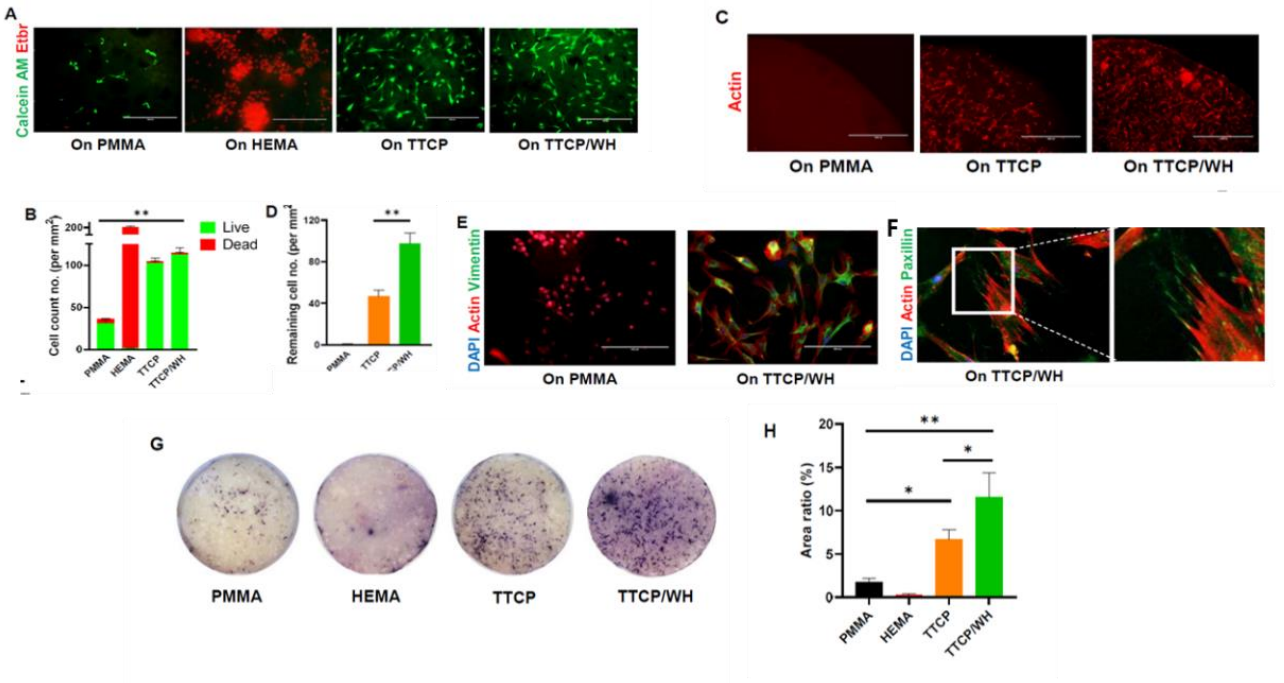

Figure 8. Focal adhesion of hBMSCs on TTCP/WH bone cement scaffolds.

A) Live/Dead assay after 24hrs of seeding hBMSCs (30000cells/scaffold) on cement scaffold. B) Live and dead cell count on cement scaffold of (A). C) Remaining cell staining with phalloidin after harsh washing of cement scaffold. D) Remaining cell count of (C). E) Actin, Vimentin and DAPI immunostaining of BMSCs after seeding on cement scaffold. F) Actin, Paxillin and DAPI staining of hBMSCs after seeding on cement scaffold. G) Alkaline phosphatase staining of BMSCs on cement scaffold after 7 days culture. H) Stained ALP area ratio of cement scaffold used in (G).

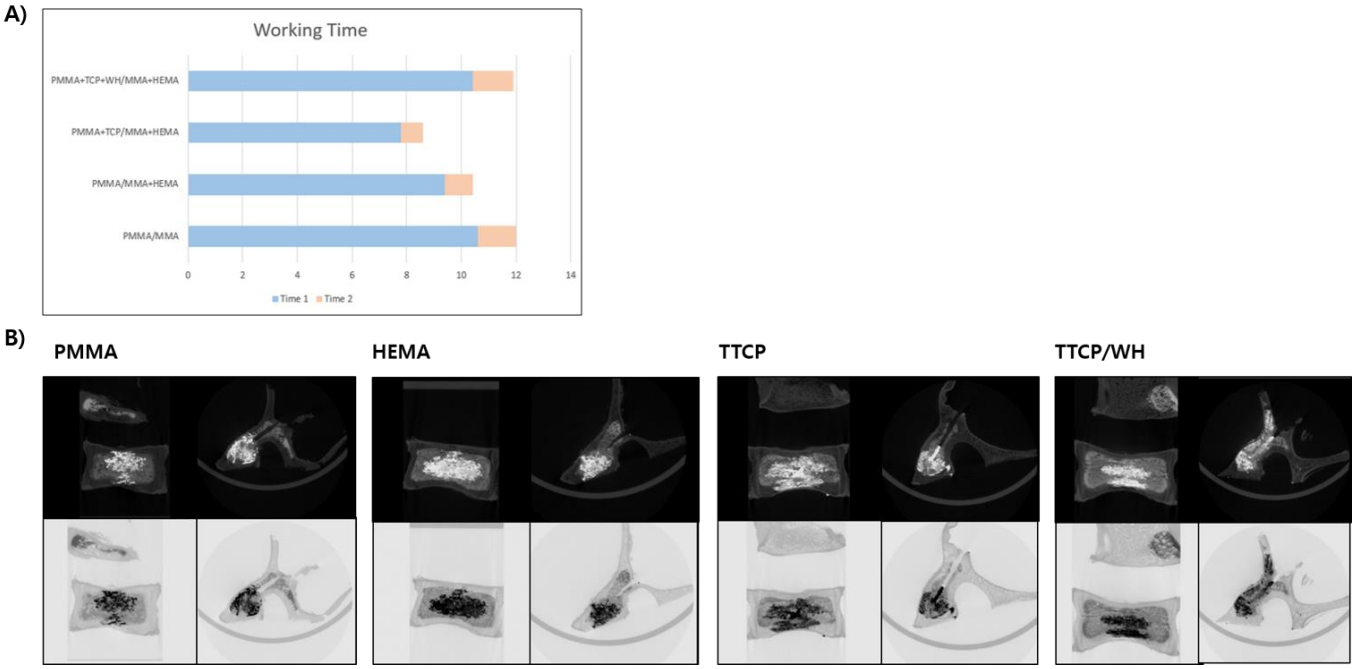

Figure 9. Operational working time and bone cement distribution in ex-vivo study.

All procedures were performed at a room temperature of 23±2℃, humidity: of 45%±5% , and VAV(Variable Air Volume): of 100%.

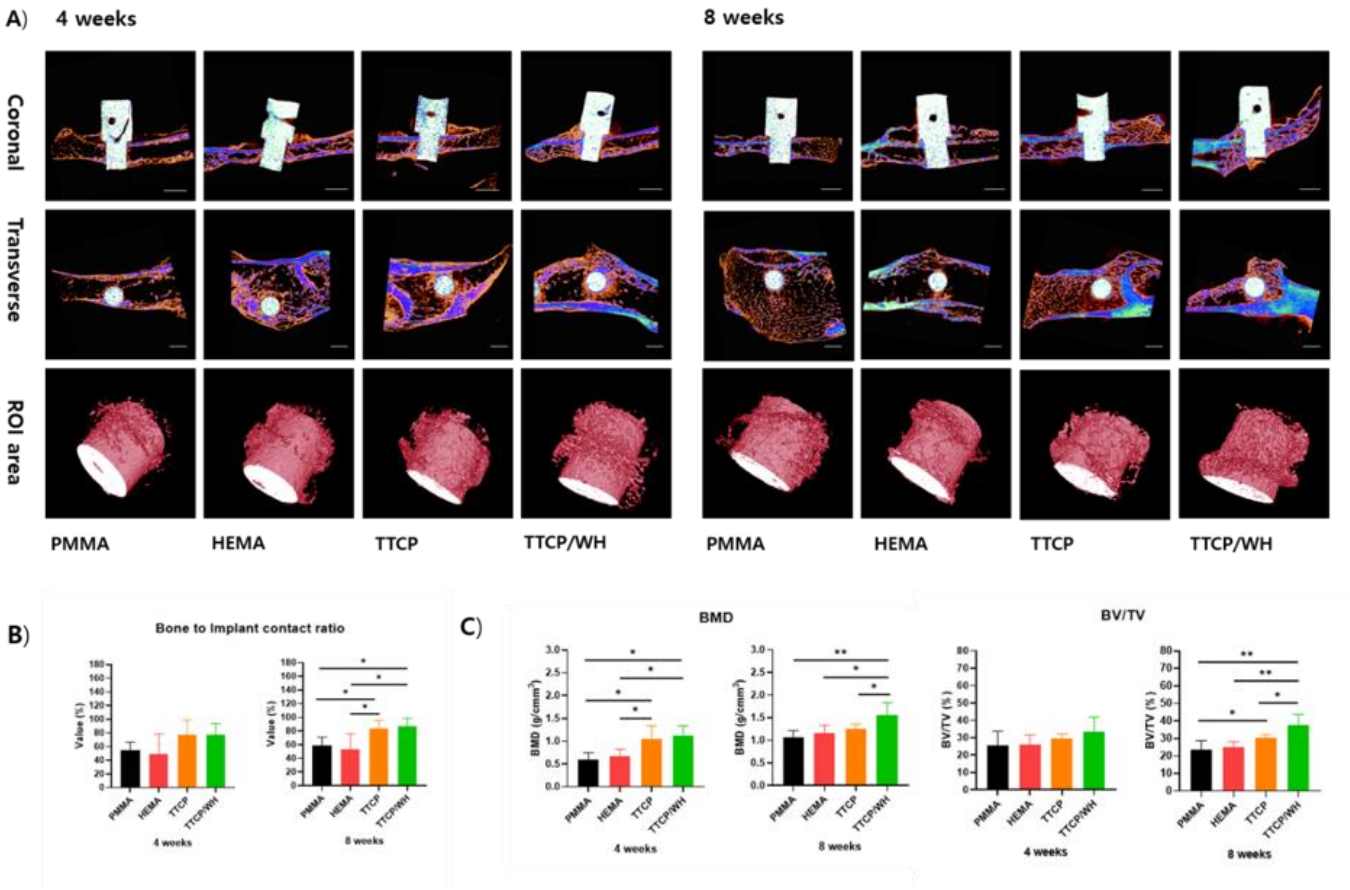

Figure 10. Micro-CT images and bone parameter outcomes.

A) Coronal and Transverse images at 4 weeks and 8 weeks post-implantation. B) Bone to implant contact ratio. C) Bone parameter quantitatively evaluation. BMD and BV/TV. (the scale bar=4 mm).

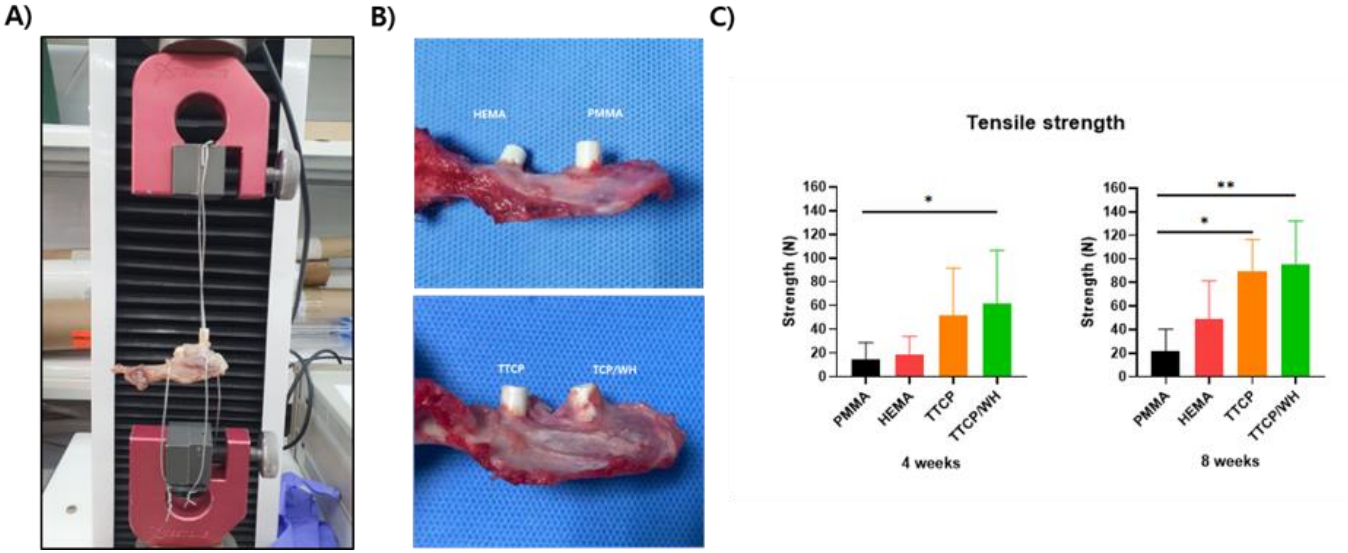

Figure 11. Biomechanical properties after implantation for 4 and 8 weeks.

A) Mechanical testing system. B) Bone regeneration around the part of the implant exposed to the iliac bone. C) Tensile strength results after implantation at 4 and 8weeks vs PMMA. (*P < 0.05 , **P < 0.001).

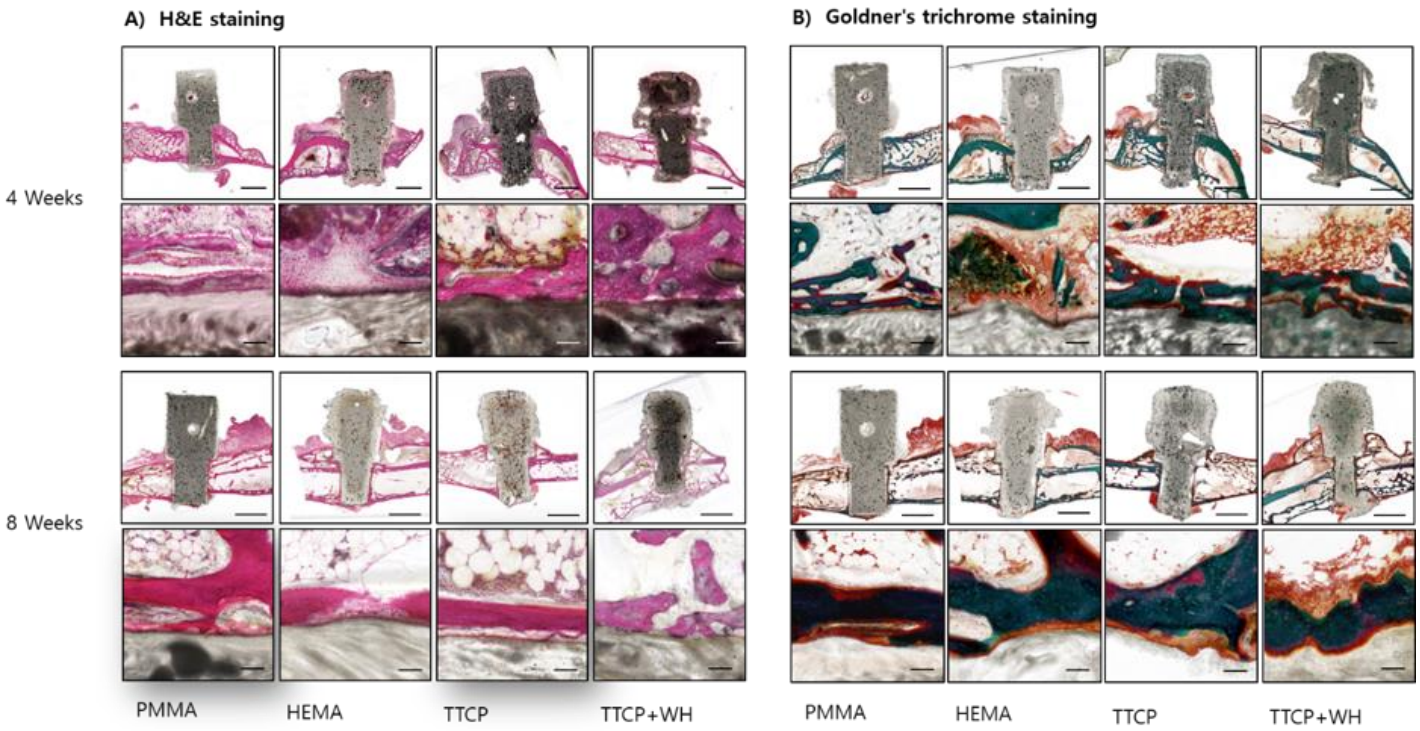

Figure 12. Histological H&E and Goldner's trichrome staining.

A) H&E staining. B) Goldner's trichrome staining. (the scale bar = 4mm and 100 μm). Implant sites at 4 weeks (sagittal plane) and 8 weeks (coronal plane) post-implantation.

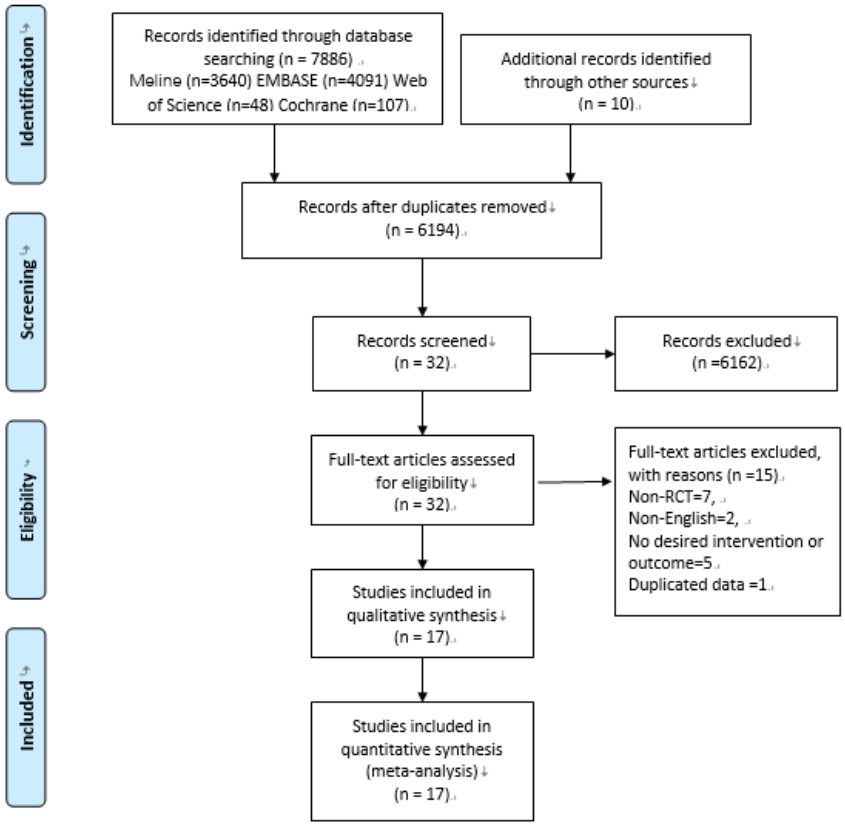

Figure 13. PRISMA flow diagram details the process of relevant clinical study selection.

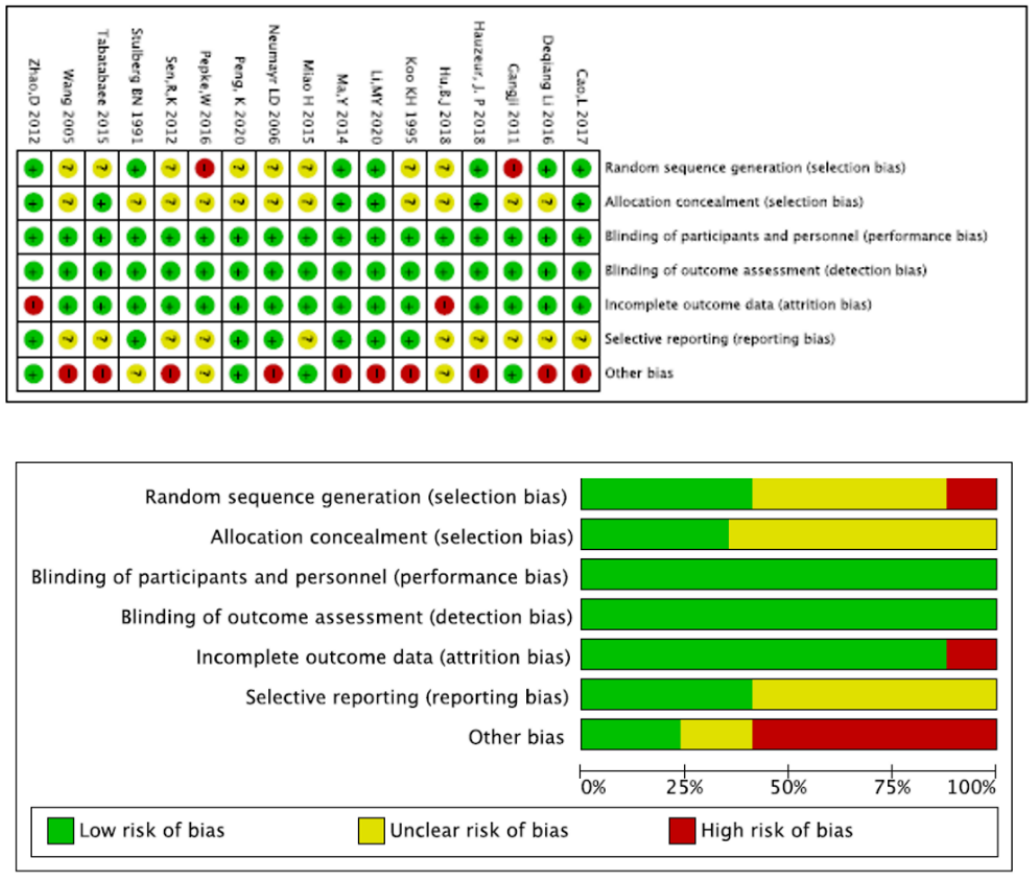

Figure 14. Details about the risk of bias assessment.

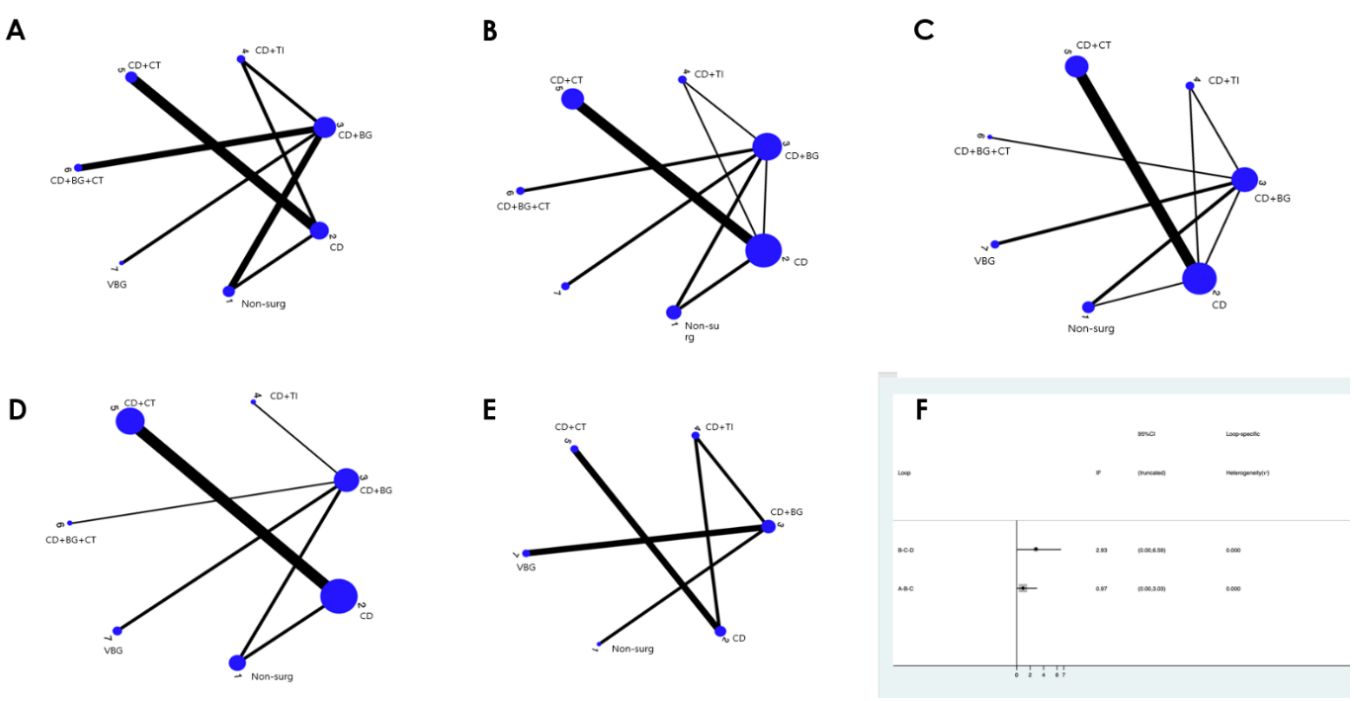

Figure 15. Network plot of the direct comparisons of the outcomes for all included studies.

A) risk factor of ONFH, B) stage 3 C) radiographic progression D) conversion to THA, E) HHS, F) the inconsistency plots of the direct and indirect comparisons, in radiographic progression.

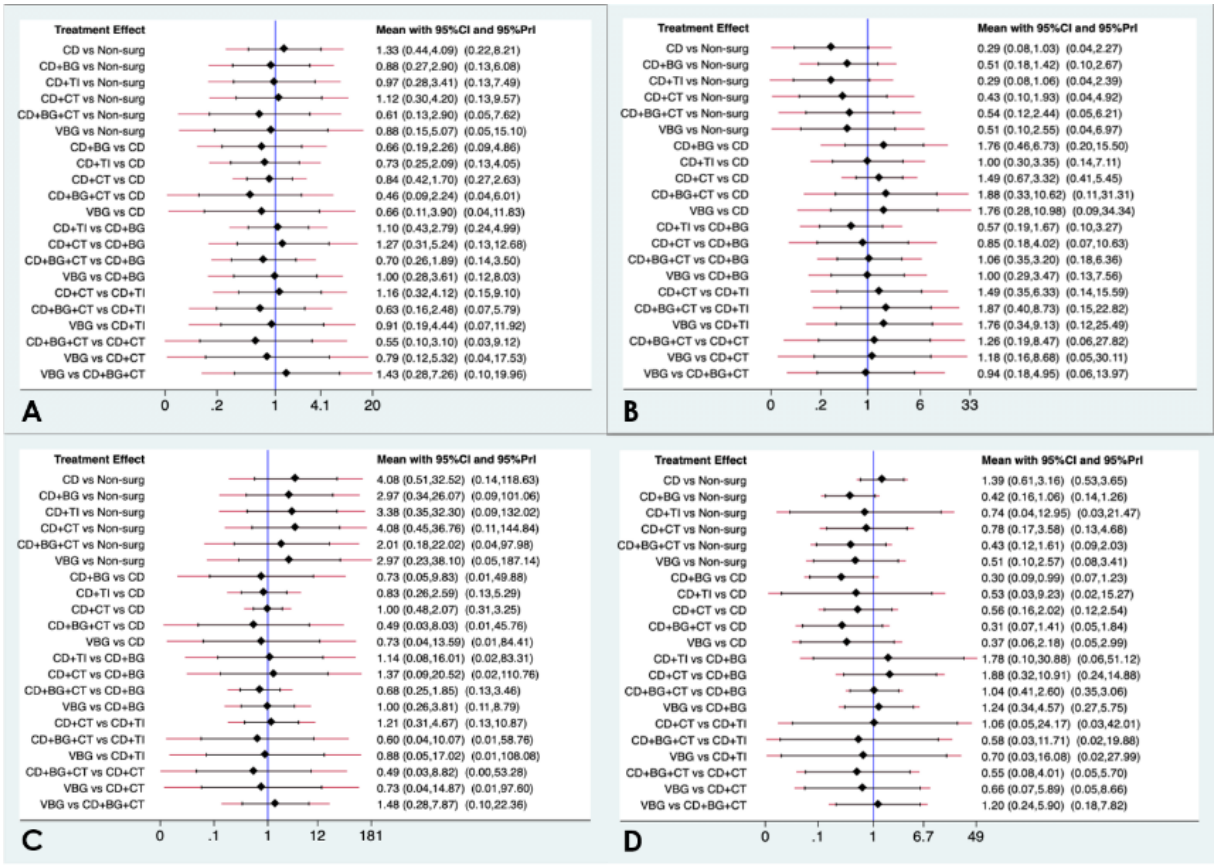

Figure 16. Confidence intervals and predictive intervals of the estimates of outcomes of risk factor of ONFH and stage 3.

A) Steroid. B) Alcohol. C) Idiopathic. D) ONFH stage 3.

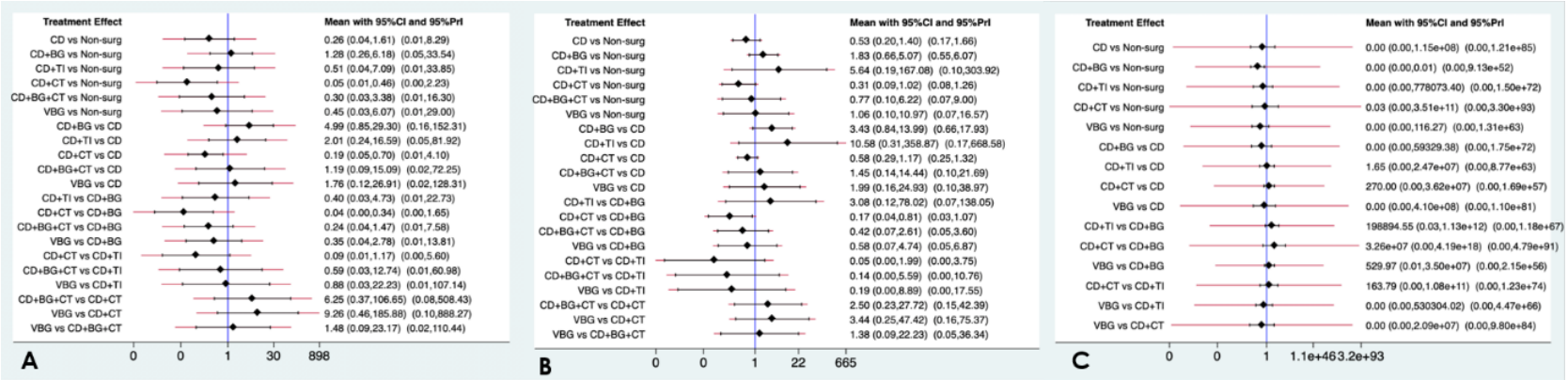

Figure 17. Confidence intervals and predictive intervals of the estimates of outcomes.

A) the rate of radiographic progression. B) the rate of conversion to THA. C) HHS.

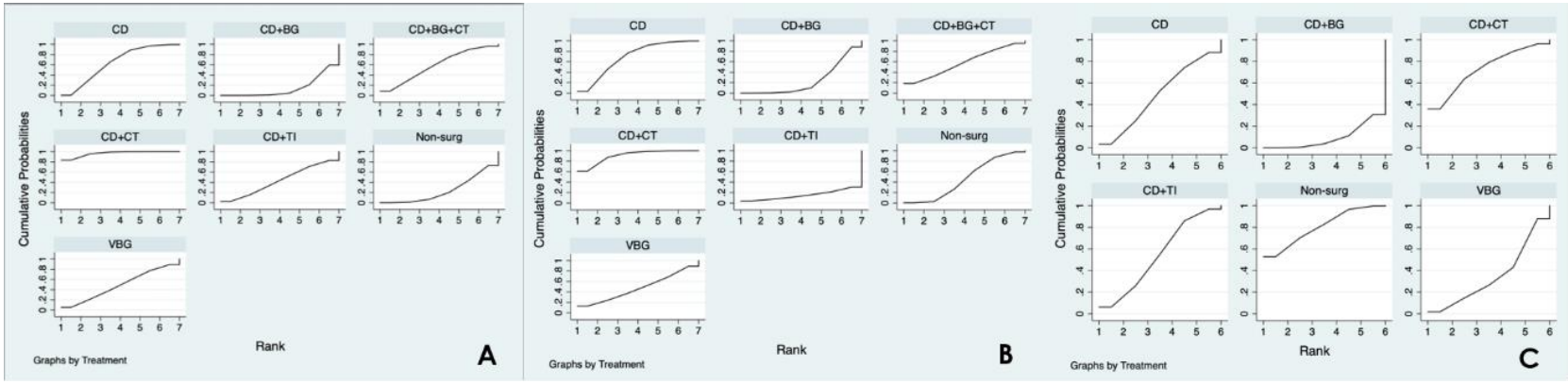

Figure 18. Cumulative ranking curve of the outcomes of each JPT method.

A) the rate of radiographic progression. B) the rate of conversion to THA. C) HHS.

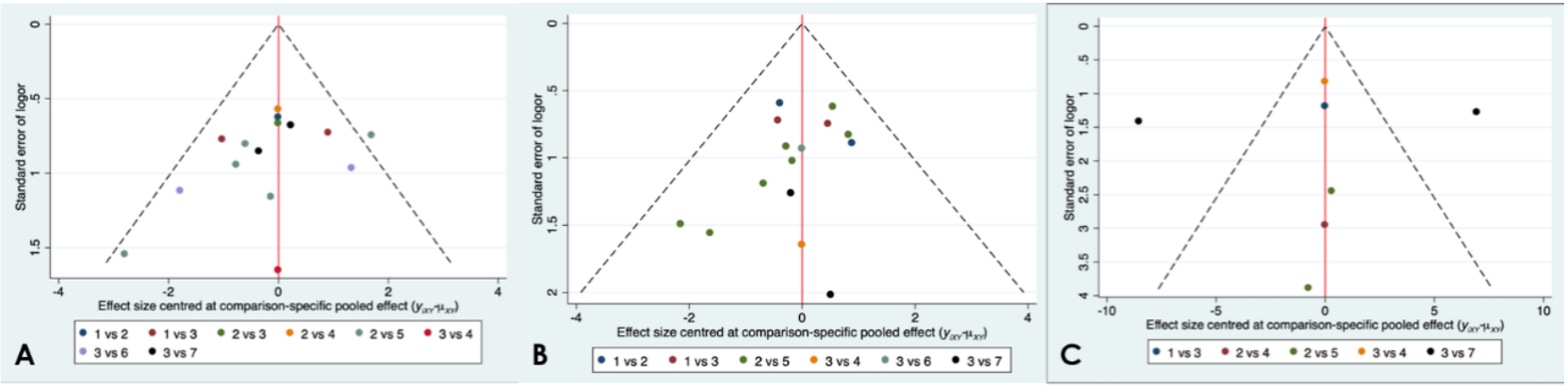

Figure 19. Comparison-adjusted funnel plots.

A) the rate of radiographic progression. B) the rate of conversion to THA. C) HHS.

1: Non-surgical treatment. 2: Core decompression (CD). 3: CD+BG. 4: CD+TI. 5: CD+CT. 6: CD+BG+CT. 7: VBG

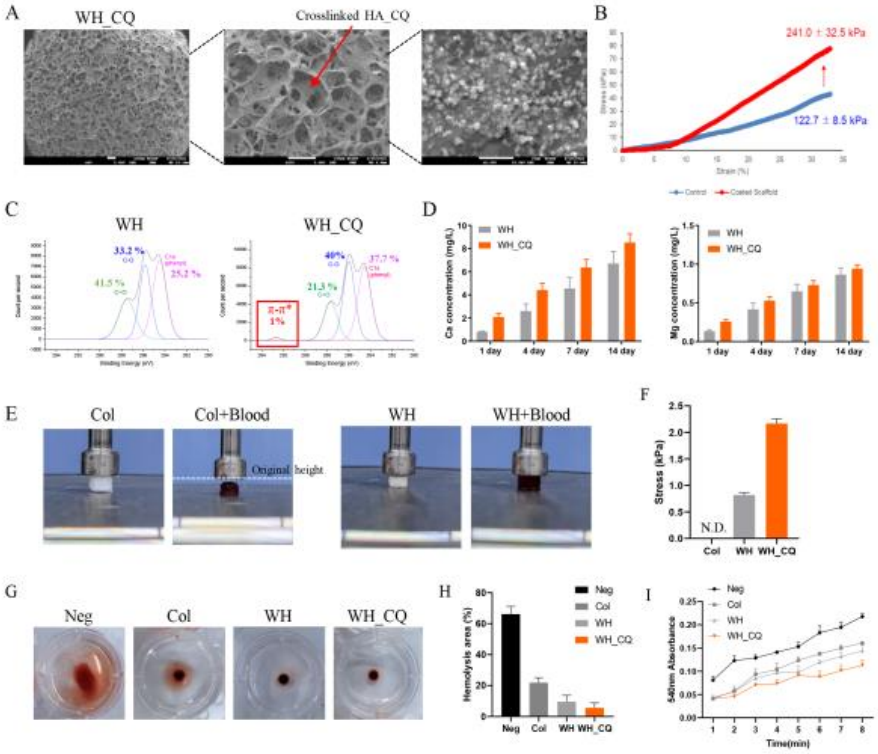

Figure 20. Characteristics of fabricated scaffold.

(A) SEM images of WH_CQ scaffold. (B) Comparing mechanical strength test. (C) XPS analysis of carbon transition in scaffold. (D) Cation release kinetic of coated and uncoated scaffold. (E) Image of scaffold swelled with blood. (F) Stress exerted by pushing force of swelled scaffold. (G) Picture of hemolysis of scaffold at 5min after coagulation (H) Graph of hemolysis area in images of (E). (I) Absorbance measurement of dissolved plasma at each time point.

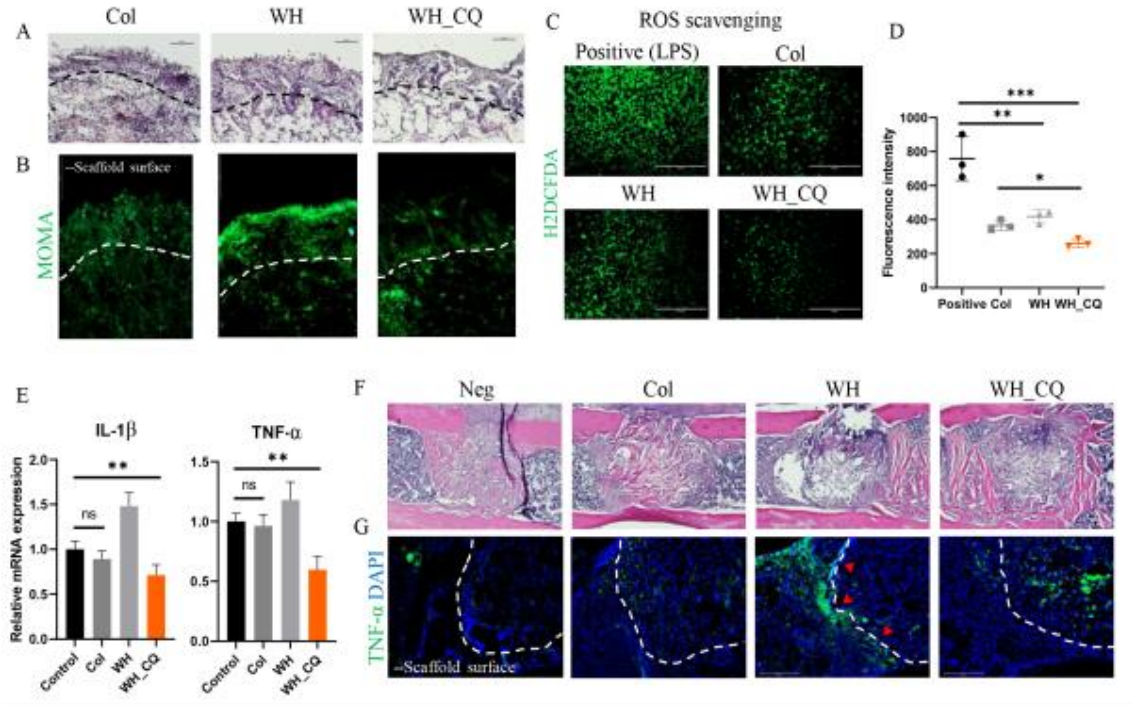

Figure 21. Anti-inflammatory effect of scaffold.

(A) H&E staining of peritoneal implanted scaffold's surface (B) Macrophage and monocyte immunofluorescence image of (A). (C) Reactive oxygen species (ROS) scavenging effect of each scaffold measured by ROS indicator H2DCFDA. (D) Measured H2DCFDA fluorescence intensity of (C). (E) Relative gene (IL-1β, TNF-α) expression normalized by GAPDH of BMDM cultured with each scaffold. (F) H&E staining images of femur bone defect after 1 week of surgery. (G) TNF-α stained femur bone defect; red arrows point to TNF-a expression at the tissue-scaffold contact. (black and white dash line indicate scaffold surface.)

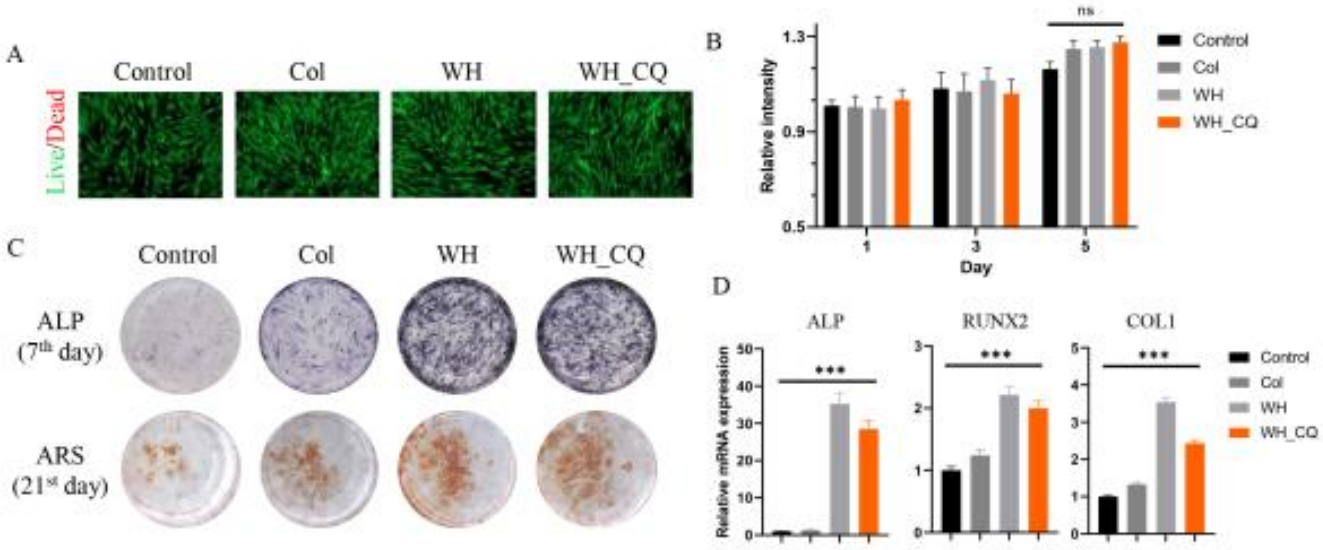

Figure 22. Biocompatibility and Osteogenic effect of Scaffold.

(A) Cell viability assay of scaffold by using live green and dead red fluorescence reagents. (B) Cell proliferation test cultured with each scaffold measured by Prestoblue. (C) Alkaline phosphatase and Alizarin red S staining of differentiated hBMSCs at day 7 and day 21. (D) Relative osteogenic gene expression of hBMSCs.

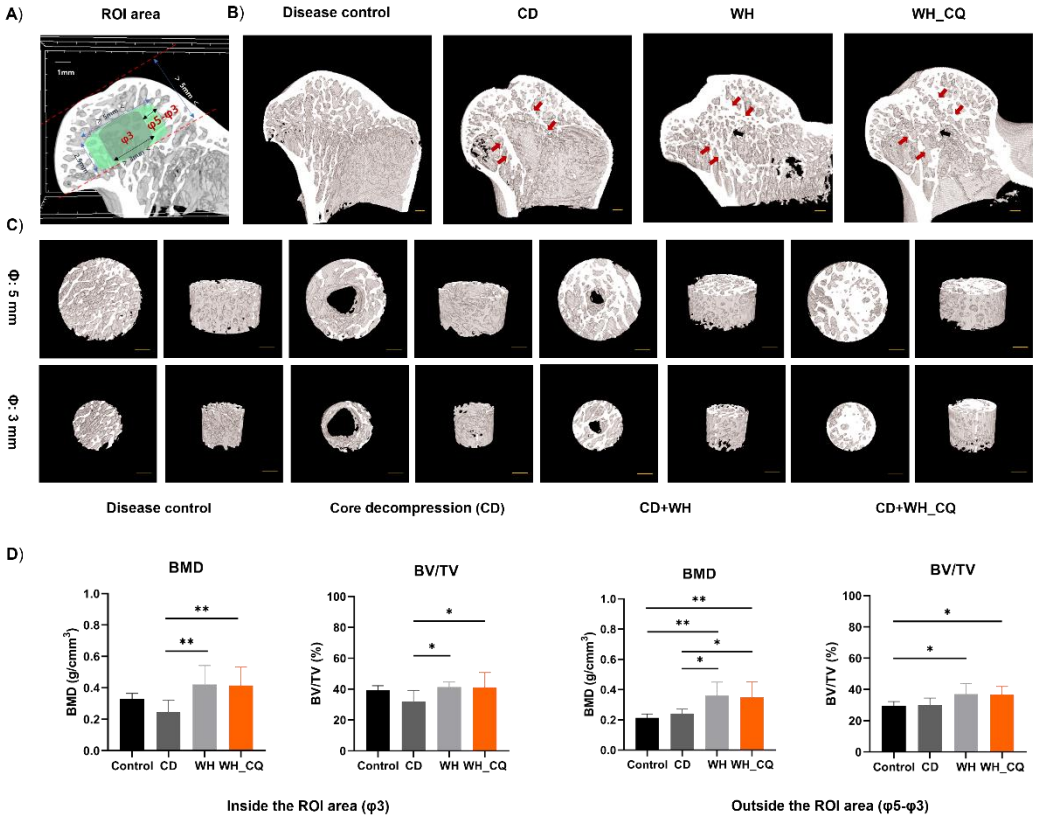

Figure 23. Micro-CT scanning and analysis.

A) Inside the ROI area: 3-mm-diameter x 2.5-mm length; Outside the area: (φ 5- φ 3)-mm x 2.5-mm length. B) The representative micro-CT reconstructive images of the proximal femur in each group. C) The representative 3-d reconstruction of ROI area images in each group. D) Bone parameter quantitatively evaluation, BMD and BV/TV. Scale bar=1 mm. *P<.05 , **<.01. BV, bone volume; TV, total volume; BMD, bone mineral density; ROI, region of interest; CD, core decompression;

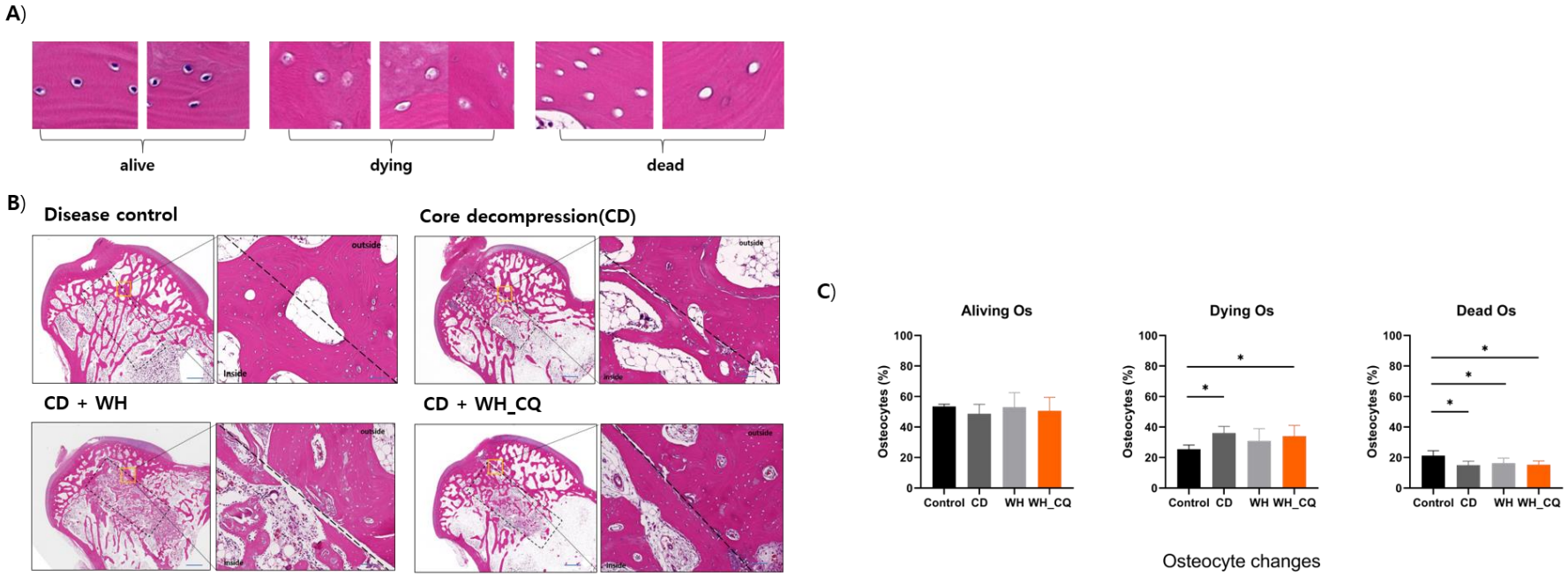

Figure 24. H&E staining photomicrographs.

A) osteocyte categories (alive, dying and dead). B) Representative H&E stained images of the femoral head and the bone tunnel boundary area. The ROI: black dashed line, scale bar=50 μm. C) osteocyte changes and their percentages (*p <.05).

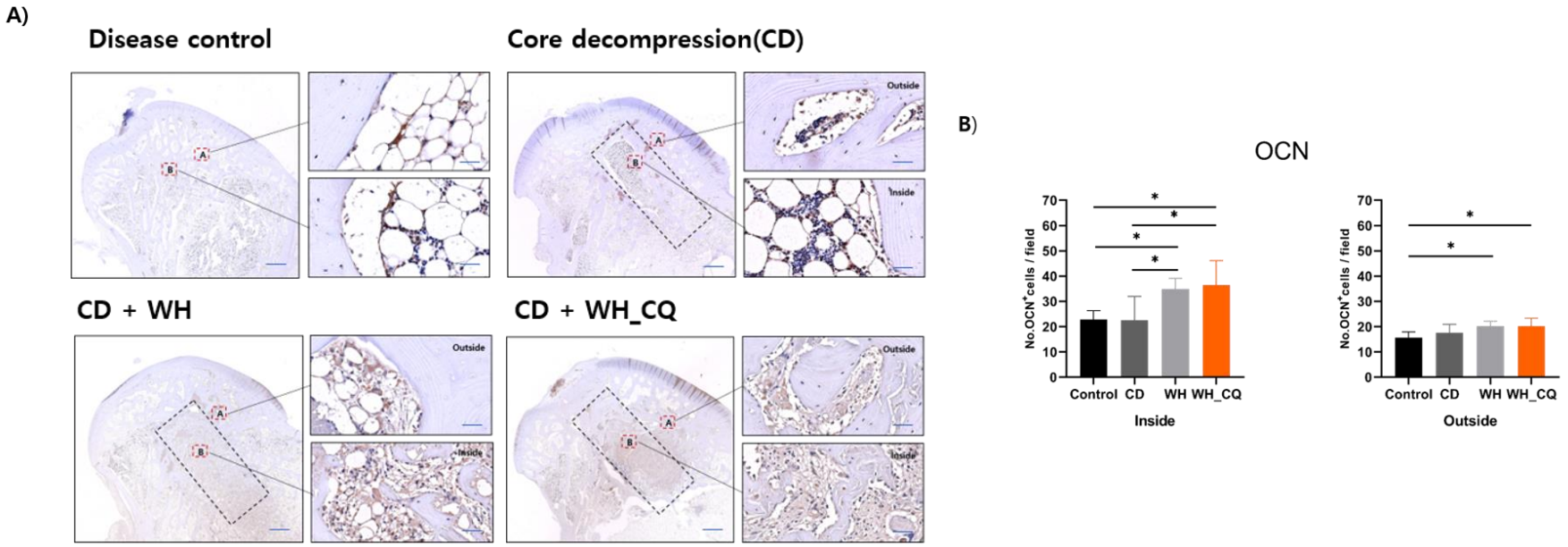

Figure 25. OCN staining photomicrographs

A) Representative OCN staining image of femoral head and ROI area. B) The number of OCN−positively stained cells inside and outside of the ROI area. The ROI: black dashed line, scale bar=50㎛(*p <.05).

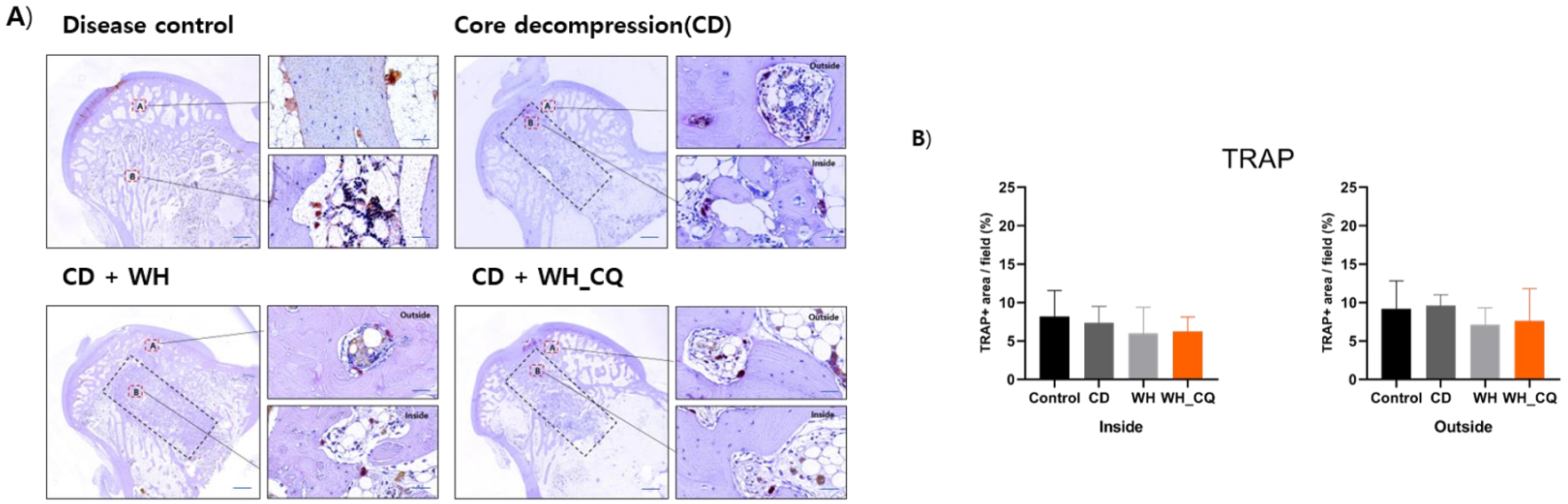

Figure 26. TRAP staining photomicrographs.

A) Representative TRAP staining image of femoral head and ROI area. B) The percentage of TRAP positive-stained area inside and outside of the ROI area. The ROI: black dashed line, scale bar=50 μm.

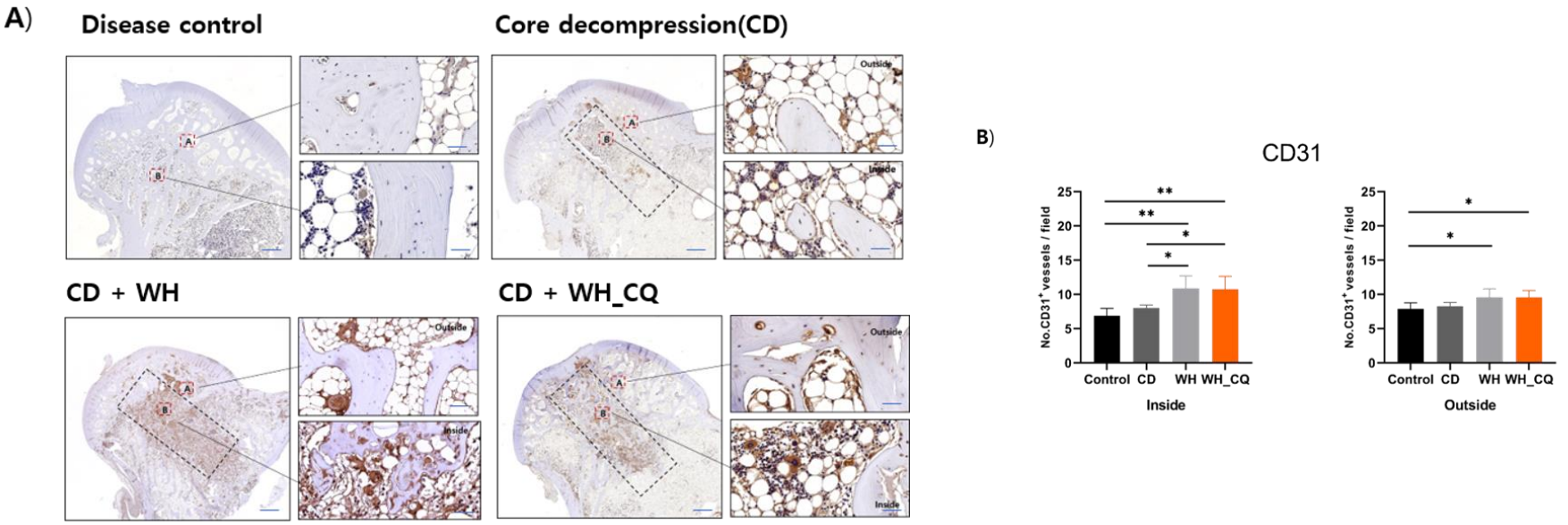

Figure 27. CD31 staining photomicrographs.

A) Representative CD31 staining image of femoral head and ROI area. B) The number of CD31-positive-stained microvessels inside and outside of the ROI area. The ROI: black dashed line, scale bar=50 μm(*p <.05).

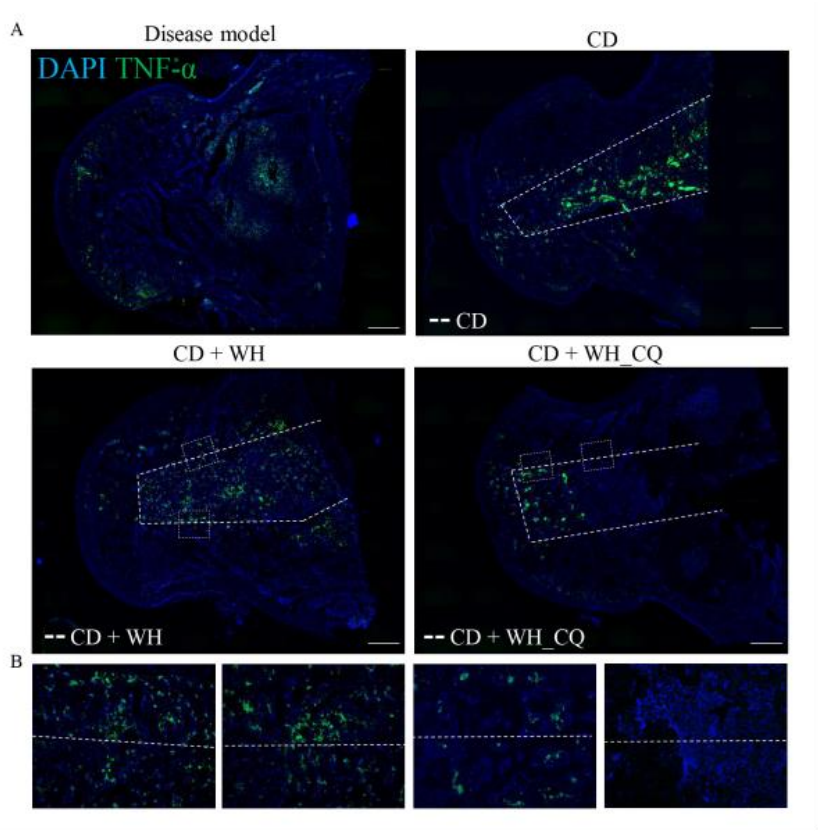

Figure 28. TNF−α staining photomicrographs

(A) Representative TNF−α staining image of femoral head; white dash line is CD or scaffold implant site. (B) Magnified images of immunostaining of TNF−α; CD+WH (left), CD+WH_CQ (right). scale bar=50μm

국문 초록

생체활성 휘트로카이트계 생체재료가 골 결손 및 괴사 모델에서 골 재생에 미치는 영향

–기능성 골시멘트와 항산화 코팅 지지체 개발에 대한 연구–

류치엔저

정형외과 전공

서울대학교 대학원

서론:

휘트로카이트(Whitlockite: Ca18Mg2(HPO4)2(PO4)12, WH)는 새로운 바이오세라믹으로서 뛰어난 장점과 가능성을 가지고 있다. 인산칼슘계 세라믹과 비교하여 WH는 화학적 조성에 칼슘, 인산이온 외에 마그네슘 이온이 포함되어 있기 때문에 골조직 재생 공학에서 더 우수한 골 재생 효과를 가지고 있다. 기존 연구에서 휘트로카이트는 하이드록시아파타이트 (Hydroxyapatite:HAP) 및 삼인산화칼슘(Tricalcium phosphate:TCP)보다 우수한 골전도성 및 골유착성을 보였고, 골 재생 촉진에 더 효과적이었다. 그러나 WH 세라믹 소재와 이를 기반으로 한 생체소재의 잠재적인 임상적 가치를 입증하기에는 전임상 연구가 아직 많이 부족한 실정이다. 따라서 본 연구에서는 특정 골질환에 대한 WH 기반 생체재료를 디자인 및 제작하고, 그의 생물학적 특성 밝히고, in vitro 및 in vivo 실험을 통해 새로운 바이오세라믹 및 생체재료로서의 응용가치와 가능성을 검증하는데 목적이 있다.

방법:

본 연구에서는 임상적으로 흔한 골질환(골다공증성 척추압박골절 및 대퇴골두 괴사)을

위해 두 가지 유형의 휘트로카이트 기반 맞춤형 생체 재료(즉 휘트로카이트 함유된 기능성 골시멘트(1부)와 항산화 코팅된 다기능 휘트로카이트 지지체(2부))를 디자인 및 제작하였다. 1부에서는 사인산칼슘(TTCP)과 휘트로카이트를 기존 PMMA 골 시멘트와 혼합하여 새로운 기능성 골시멘트를 제작하였고 그에 대한 기계적 물성, 작업 가능한 시간 등 특성에 대해 국제 표준화 기구 규격(ISO 5833)을 참고로 하여 체계적으로 평가분석하였다. 그리고 생체 외 및 생체 내 연구를 통해 생체적합성, 골전도성, 골유합 능력을 평가하였다. 2부에서는 먼저 PRISMA-NMA(Preferred Reporting Items for Systemic Reviews and Meta-analysiss for Network Meta-analysis) 보고 가이드라인에 따라 대퇴골두 괴사에 대한 다양한 조기 치료방법에 대한 통계 분석을 수행하여 그 유효성을 평가 분석하였다. 그런 다음 ImTYR(tyrosinase immobilized glass bead) 시스템을 사용하여 대퇴골두 괴사를 치료하기 위한 항산화제 다기능 휘트로카이트 지지체를 디자인 및 제작하였다. 그리고 생체재료의 물리화학적 특성을 체계적으로 평가하였고 생체 외 연구 및 스테로이드 유도 토끼 대퇴골두 괴사 모델에서의 생체 내 연구를 통해 생물학적 특성을 평가하였다.

결과:

1 부: TTCP/WH 골 시멘트는 ISO 5833 표준에 부합하였고 임상에서 사용하기 적합한 작업 시간을 보였으며, 기존 PMMA보다 Young's modulus가 낮았다. In vitro 실험에서는 TTCP/WH 골 시멘트는 PMMA에 비해 양호한 생체적합성과 골 형성 활성 및 골 형성 관련 유전자 발현이 향상된 것으로 나타났다. 또한 토끼 장골 결손 연구에서는 보다 뚜렷한 골 재생 능력과 골 유착 능력을 보였다.

2 부: 네트워크 메타분석 결과 대퇴골두 괴사에서 방사선학적 진행(radiographic progression), 고관절 전치환술(THA)로의 전환 및 Harris Hip Score(HHS) 값에서는 기존 조기 치료법들이 통계적으로 차이가 없었다. 다만 핵심 감압술+세포치료법이 방사

선학전 진행 결과에서 상대적으로 보다 좋은 결과를 보였다. WH를 포함하는 골전도 지지체는 ImTYR 시스템을 사용하여 항산화제 HA_CQ로 코팅 되었다. In vitro 연구에서는 WH와 WH_CQ는 hBMSC 세포에 대한 골 형성 활성 효과와 관련 유전자의 발현을 대조군이나 콜라겐 그룹에 비해 향상시키는 것으로 나타났다. 스테로이드를 투여한 ONFH 토끼 모델에서 WH와 WH_CQ는 단순 감압술 보다 더 뚜렷한 골 재생 및 미세혈관 재생 능력을 보였고, 파골세포를 억제하는 것이 확인되었다. 뿐만 아니라 WH_CQ 군은 기타 군과 비교 시 ROS 감소 효과 그리고 전 염증 사이토카인 발현(pro-inflammation cytokine expression)을 감소시키는 작용을 관찰할 수 있었으며 이는 골괴사 질병 진행 지연에 긍정적인 영향을 주는 것으로 나타났다

결론:

TTCP/WH 기능성 골 시멘트는 우수한 생체적합성과 골 전도성 그리고 골 형성 촉진 능력으로 추후 골다공성 척추 압박 골절을 치료함에 있어서 보다 좋은 생체재료로서 활용이 기대된다. 항산화 코팅된 다기능 휘트로카이트 스캐폴드는 WH의 고유한 생물학적 특성을 보유해 골 재생 능력이 뛰어나고 미세혈관 생성 촉진 작용과 더불어 ROS 감소 및 전 염증 사이토카인 발현(pro-inflammation cytokine expression) 감소 효과를 보이고 있어 이는 향후 조기 대퇴골두 괴사의 치료에 사용될 수 있을 것으로 기대된다.

본 연구의 결과는 WH 세라믹 기반 생체재료에 대한 더 깊은 이해와 실험적 기초를 제공하는데 의의가 있으며, WH는 추후 의학 영역에 광범위하게 사용될 것으로 예상된다.

주요어: 휘트로카이트; 바이오세라믹, 골격계 질환; 생체재료, 골 대체재;

학번: 2020-35192